2012

A modeling study on the response of Chesapeake Bay to hurricane events of Floyd and Isabel

KH Cho
Virginia Institute of Marine Science

Harry V. Wang
Virginia Institute of Marine Science

Jian Shen
Virginia Institute of Marine Science

A Valle-Levinson

YC Teng

Ocean Modelling 49–50 (2012) 22–46

Contents lists available at SciVerse ScienceDirect

Ocean Modelling

journal homepage: www.elsevier.com/locate/ocemod

A modeling study on the response of Chesapeake Bay to hurricane events of Floyd and Isabel

Kyoung-Ho Cho [a,b], Harry V. Wang [a,*], Jian Shen [a], Arnoldo Valle-Levinson [c], Yi-cheng Teng [a]

[a] Virginia Institute of Marine Science, College of William and Mary, Gloucester Point, VA, United States
[b] Center for Coastal Margin Observation and Prediction, Oregon Health and Science University, Portland, OR, United States
[c] Department of Civil and Coastal Engineering, University of Florida, Gainesville, FL, United States

ARTICLE INFO

Article history:
Received 24 October 2011
Received in revised form 5 February 2012
Accepted 27 February 2012
Available online 14 March 2012

Keywords:
Barotropic/baroclinic response
Chesapeake Bay
Hurricane events
Oceanic salt flux
Storm surge
Wind-induced vertical mixing
Wind-induced straining
Destratification/restratification

ABSTRACT

The response of Chesapeake Bay to forcing from two hurricanes is investigated using an unstructured-grid three-dimensional hydrodynamic model SELFE. The model domain includes Chesapeake Bay, its tributaries, and the extended continental shelf in the mid-Atlantic Bight. The hurricanes chosen for the study are Hurricane Floyd (1999) and Hurricane Isabel (2003), both of which made landfall within 100 km of the mouth of the Bay. The model results agree reasonably well with field observations of water level, velocity, and salinity. From the Bay's water level response to the hurricanes, it was found that the storm surge in the Bay has two distinct stages: an initial stage set up by the remote winds and the second stage – a primary surge induced by the local winds. For the initial stage, the rising of the coastal sea level was setup by the remote wind of both hurricanes similarly, but for the second stage, the responses to the two hurricanes' local winds are significantly different. Hurricane Floyd was followed by down-Bay winds that canceled the initial setup and caused a set-down from the upper Bay. Hurricane Isabel, on the other hand, was followed by up-Bay winds, which reinforced the initial setup and continued to rise up against the head of the Bay. From the perspective of volume and salt fluxes, it is evident that an oceanic saltwater influx is pushed into the Bay from the continental shelf by the remote wind fields in the initial stages of the storm surge for both Floyd and Isabel. In the second stage after the hurricane made landfall, the Bay's local wind plays a key role in modulating the salinity and velocity fields through vertical mixing and longitudinal salt transport. Controlled numerical experiments are conducted in order to identify and differentiate the roles played by the local wind in stratified and destratified conditions. Down-estuary local wind stress (of Hurricane Floyd-type) tends to enhance stratification under moderate winds, but exhibits an increasing-then-decreasing stage when the wind stress increases. The up-estuary local wind stress (of Hurricane Isabel-type) tends to penetrate deeper into the water column, which reduces stratification by reversing gravitational circulation. To characterize mixing conditions in the estuary, a modified horizontal Richardson number that incorporates wind stress, wind direction, horizontal salinity gradient, and vertical eddy viscosity is used for both hurricanes. Finally, the direct precipitation of rainfall into the Bay during Hurricane Floyd appears to create not only a thin surface layer of low salinity but also a seaward barotropic pressure gradient that affects the subsequent redistribution of salinity after the storm.

1. Introduction

The Chesapeake Bay (CB), located near the mid-Atlantic Bight along the US East Coast, is a partially mixed estuary and the largest in the United States. The Bay is approximately 320 km long from its entrance to its head at the mouth of the Susquehanna River. Its width varies from a few kilometers in the Northern Bay to 20 km at the Bay mouth with its widest point, just south of the Potomac River mouth, spanning 45 km (Fig. 1). CB is a complicated estuarine system with shorelines exceeding 7000 km that is comprised of many sub-estuaries and that allows discharge from approximately fifty tributaries. The total freshwater inputs to the CB system are on the averages of 2570 $m^3 s^{-1}$, derived predominantly from the northern and western shores, with a small portion entering from the eastern shore; the most notable of these are the Susquehanna, Patuxent, Potomac, Rappahannock, York, James, and Choptank Rivers. Nearly the same amount of seawater as freshwater outflow enters the Bay through the entrance from the mid-Atlantic Bight shelf waters (Boicourt, 1973; Wang and Elliott, 1978; Valle-Levinson, 1995). These exchange processes at the mouth of CB are influenced by astronomical tides, atmospheric forcing, buoyancy forcing, and bathymetric features (Valle-Levinson and Lwiza, 1997; Valle-Levinson and Wilson, 1994; Valle-Levinson et al., 2001, 2002,

* Corresponding author. Tel.: +1 8046847215; fax: +1 8046847899.
E-mail address: wang@vims.edu (H.V. Wang).

1463-5003
http://dx.doi.org/10.1016/j.ocemod.2012.02.005

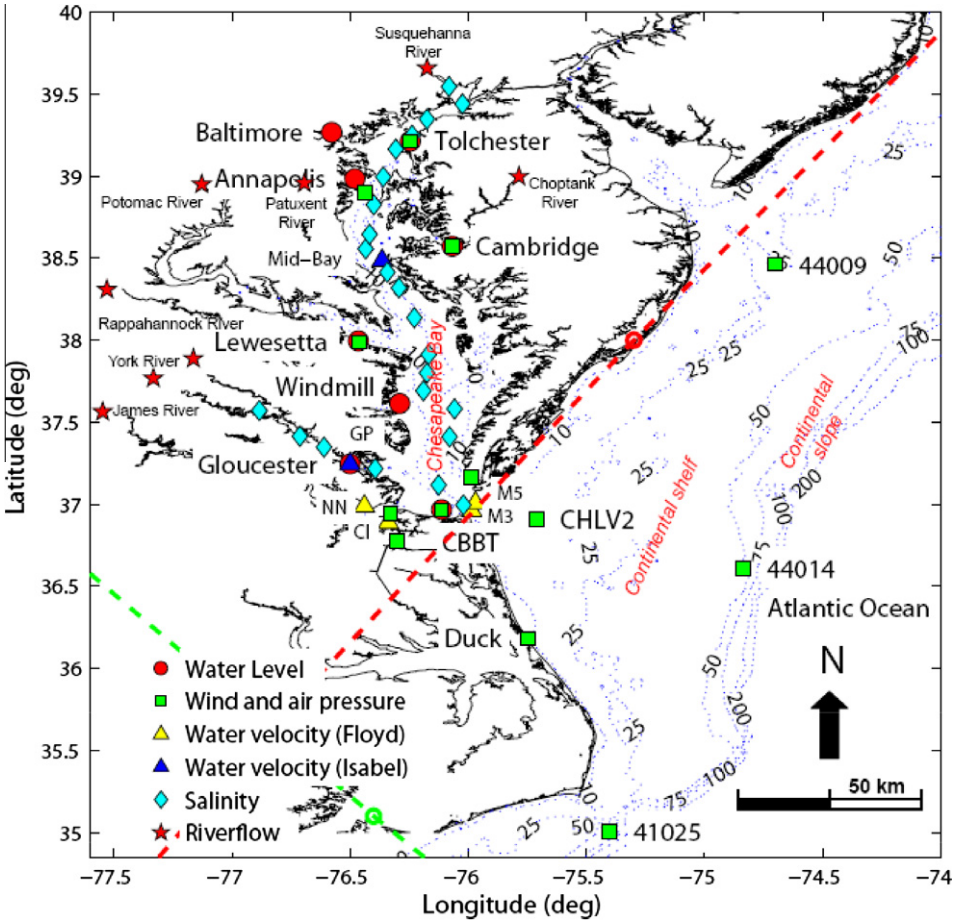

Fig. 1. A map of Chesapeake Bay observation station locations with bathymetric soundings (meters). Red circles represent water elevation data; green squares represent wind data; triangles represent current data (red: Year 1999; blue: Year 2003); cyan diamonds represent salinity data; and red stars represent riverflow. Red and green dashed lines represent the tracks of Hurricanes Floyd and Isabel, respectively.

2003). The mean rate of exchange between the ocean and the Bay is approximately 8×10^3 m^3 s^{-1} (Austin, 2002).

Within our recent history, CB was hit by two tropical cyclones, Hurricane Floyd in 1999 and Hurricane Isabel in 2003, both of which made landfall in North Carolina as Category 2 hurricanes (Table 1). These two hurricanes had ambivalent tracks (Fig. 2): Floyd's track was nearly parallel to the coast, corresponding to an eastern-type storm, whereas Isabel's track was perpendicular to the coast, corresponding to a western-type storm. Eastern-type hurricanes that travel to the east of the Bay generate a maximum surge in the southern portion of the Bay, whereas western-type hurricanes that pass to the west of the Bay create the highest surge in the northern part of the Bay (Pore, 1960, 1965; Wang et al., 2005; Shen et al., 2005, 2006a,b). The response of the Bay to a moving hurricane is characterized by volume and salt influxes from the ocean initiated by remote winds, locally wind-induced vertical mixing, buoyancy effects induced by heavy rains, and freshwater inflows under gravitational circulation, and are accompanied by storm-induced barotropic/baroclinic flow motions (Valle-Levinson et al., 1998, 2002). When winds are intensified, the magnitude of wind-driven circulation frequently exceeds that of the gravitational circulation (Goodrich et al., 1987). Goodrich et al. (1987) observed that wind-induced destratification in CB frequently occurred from early autumn through mid-spring. Recently, Li et al. (2007) explored the hurricane-induced destratification and post-storm restratification processes in CB during Hurricane Isabel. They suggested that the combined remote and local wind forcing can cause different effects on turbulent mixing and, after the

Table 1
Some comparative aspects of Hurricanes Floyd and Isabel.

Name/Aspects	Hurricane Floyd	Hurricane Isabel
Date	September 7–17, 1999	September 6–19, 2003
Landfalling location	North Carolina	North Carolina
Landfalling category (maximum)	Category 2 (4)	Category 2 (5)
Maximum wind speed and minimum pressure	154 mph, 921 mb	161 mph, 920 mb
Pore's classification	Eastern	Western
Maximum storm surge in CB	1. 559 m (Money Point, VA)	2.487 m (Chesapeake City, MD)
Total rainfall onto CB (max)	10–15 inches	1–2 inches
Total river flows	291 billion gallons (September 16–22; USGS)	1190 billion gallons (September 19–25; USGS)
Damage Estimates	$ 4.5 billion (particularly NC)	$ 3.6 billion ($ 2.67 billion both VA and MD)

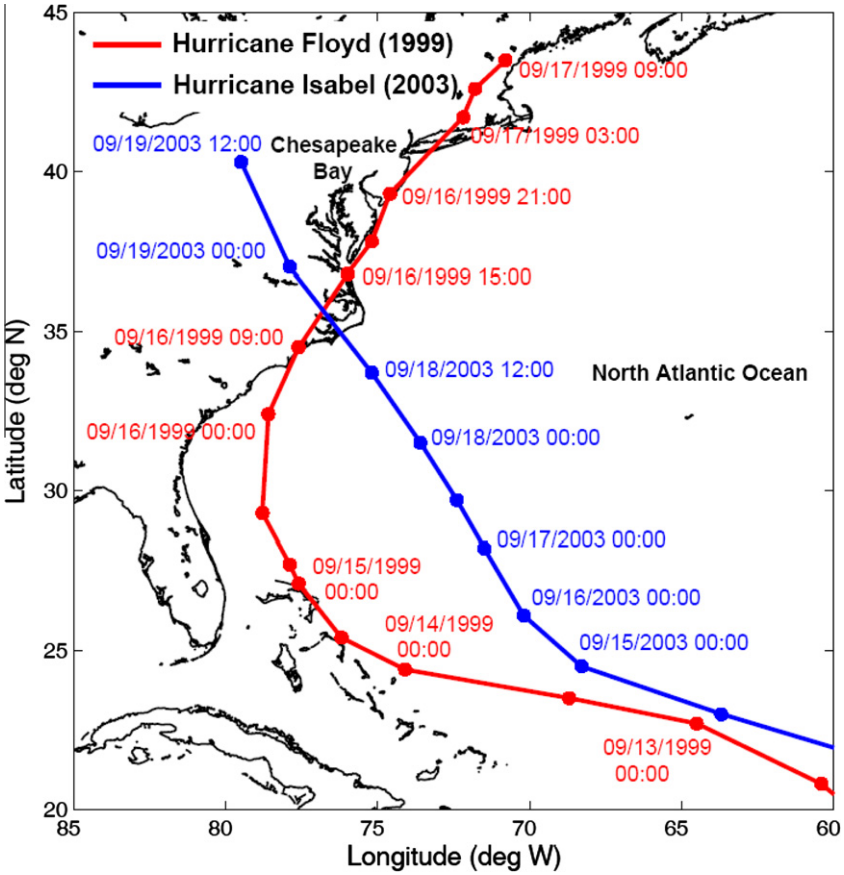

Fig. 2. Tracks of Hurricanes Floyd (red) and Isabel (blue).

hurricane passes, turbulent mixing due to tides or subsequent winds works against the gravitational adjustment to produce a quasi-steady salinity distribution in the Bay. Guo and Valle-Levinson (2008) found that the effect of remote winds was dominant over that of local winds on volume transports at the Bay entrance. Wind directions are thought to play a significant role, as illustrated by Guo and Valle-Levinson (2008) and Chen and Sanford (2009) (hereafter referred to as CS). Wind stress increases estuarine stratification by reducing the longitudinal density gradient (Geyer, 1997; North et al., 2004; Scully et al., 2005). Geyer (1997) showed that down-estuary winds enhanced surface outflow, significantly reducing the along-estuary salinity gradient. North et al. (2004) demonstrated that increased stratification was associated with down-estuary wind events, but did not address the role that the increased stratification may play in reducing vertical mixing and enhancing the baroclinically driven estuarine circulation. In their investigation of Virginia's York River Estuary, Scully et al. (2005) found that down-estuary winds enhance the tidally averaged vertical shear, which interacts with the along-channel density gradient to increase vertical stratification, whereas up-estuary winds tend to reduce, or even reverse, the vertical shear, reducing vertical stratification, called *wind-induced straining*. Wind stress not only plays a predominant role in mixing away estuarine stratification, but also acts to strain the along-channel estuarine density gradient. In a partially mixed estuary system, down-estuary winds tend to enhance tidally averaged vertical shear, increasing vertical stratification, whereas up-estuary winds tends to reduce or reverse vertical shear, decreasing vertical stratification. During the passage through CB of Hurricane Floyd (1999) and Hurricane Isabel (2003) through CB, very different wind patterns are generated – Hurricane Floyd was followed by northerly (down-estuary) winds whereas Hurricane Isabel was followed by southerly (up-estuary) winds. Despite the unsteadiness of the hurricane wind initially, the post-storm winds were quite persistent based on the hurricane track relative to the orientation of the Bay. This provides a natural testbed for conducting twin experiments in investigating the effects of the wind – both its direction and speed – on the vertical stratified-destratified dynamics of the Bay.

Furthermore, Valle-Levinson et al. (2002) documented the influence of intense rains from consecutive tropical storms, Dennis and Floyd, and the wind forcing from Floyd on net transport at the Bay entrance. They proposed that the barotropic pressure gradient associated with the precipitation and the wind-induced sea level slopes overwhelmed the baroclinic pressure gradient to produce a bidirectional flow. From a numerical modeling context, it is worthwhile here to test the hypothesis proposed and quantify the effect of precipitation which falls directly onto the Bay during the hurricane.

The purpose of this study, therefore, is to examine the response of CB to hurricane events by comparing two ambivalent hurricanes, Floyd and Isabel. The first goal is to estimate the amount of saltwater transport and its pattern in CB during the hurricanes, the second goal is to obtain further insight into the physics of storm-induced vertical mixing in the Bay, and the final goal is to verify the influence of precipitation on transport at the Bay entrance proposed by Valle-Levinson et al. (2002).

2. The observation data collected during Hurricanes Floyd and Isabel

Making observations during hurricanes is technically difficult. During two hurricane events in CB, five categories of data survived

and were assembled from various resources for analysis. They are: (1) tidal records from 16 locations, (2) time series of water velocity from two locations, (3) time series of surface and bottom salinity data from two locations, (4) wind and atmospheric pressure data, and (5) river stream flow data. The measurement locations are shown in Fig. 1.

The water levels were measured at the National Oceanic Atmospheric Administration (NOAA)/ National Water Level Observation Network (NWLON) stations, which are detailed in Table 2. Each station provides two types of water level data: observed water level and predicted water level (astronomical tide). The storm surge is the difference between the two.

During Hurricane Floyd, the NOAA Current Observation Program (COP) was operating two Acoustic Doppler Current Profiler (ADCP) current meters in the lower James River estuary (Zervas et al., 2000), the Chesapeake Bay Observing System (CBOS) was measuring currents at 2.4 and 10.4 m depths at the mid-Bay buoy, and a team from Old Dominion University (ODU) was collecting water velocity data at the entrance to CB (Valle-Levinson et al., 2002).

During Hurricane Isabel, two current meters were successfully operated. One was the Aanderaa RCM-9 current meter in the mid-Bay CBOS, deployed by a team from the University of Maryland (UM) at 2.4 and 10.4 m (Boicourt, 2005; Roman et al., 2005). The other dataset was collected by the Virginia Institute of Marine Science (VIMS) from York River using a 600 kHz ADCP. This provided high-quality data on waves, storm surge, currents, and acoustic backscatter throughout the water column before, during, and after the storm (Brasseur et al., 2005; Reay and Moore, 2005).

During Hurricane Floyd, salinity data were collected by ODU from the mouth of CB at the same locations that the ADCPs and S4 were deployed (Table 2). The salinity data from mid-water and bottom depth at station M5 and the surface salinity at station M3 were low-passed using the 34-h Lanczos filter to obtain the sub-tidal record. As for other datasets, the Chesapeake Bay National Estuarine Research Reserve (CBNERR) measured surface salinity at two stations, Taskinas Creek and Clay Bank in the York River (YR), VA. During Hurricane Isabel, salinity was measured by YSI-6600 Sondes operated by CBNERR at fixed stations at Sweet Hall, Taskinas Creek, Clay Bank, and Goodwin Islands in the YR.

Meteorological data were collected from a total of 13 stations around CB operated by NOAA and the National Data Buoy Center (NDBC). Typically, wind data were taken at a height of 10 m above mean sea level (MSL) and atmospheric pressures were observed at MSL. River stream flow data from CB tributaries were obtained from the US Geological Survey (USGS) for both hurricanes (Table 3).

3. The model and external forcing

3.1. Hydrodynamic model

The baroclinic circulation in CB was performed using the semi-implicit Eulerian–Lagrangian Finite Element (SELFE) model, a free

Table 2
Station information and availability of observations during Hurricanes Floyd and Isabel in MD, DC, VA, and NC.

Station ID	Station Name	Coordinates		Observations*			
		Latitude (N)	Longitude (W)	WL	WD	WV	S
NOAA							
8570283	Ocean City Inlet, MD	38° 19.7'	75° 05.5'	X			
8571892	Cambridge, MD	38° 34.4'	76° 04.1'	X	X		
8573364	Tolchester Beach, MD	39° 12.8'	76° 14.7'	X	X		
8574680	Baltimore, MD	38° 16.0'	76° 34.7'	X			
8575512	Annapolis, MD	38° 59.0'	76° 28.8'	X			
8577330	Solomons Island, MD	38° 18.0'	76° 27.1'	X			
8594900	Washington, DC	38° 52.4'	77° 01.3'	X			
8632200	Kiptopeke Beach, VA	37° 10.0'	75° 59.3'	X	X		
8635150	Colonial Beach, VA	38° 15.1'	76° 57.6'	X			
8635750	Lewisetta, VA	37° 59.2'	76° 27.8'	X	X		
8636580	Windmill Point, VA	37° 36.9'	76° 17.4'	X			
8637624	Gloucester Point, VA	37° 14.8'	76° 30.0'	X			
8638610	Sewells Point, VA	36° 56.8'	76° 19.8'	X	X		
8638863	Chesapeake Bay BT, VA	36° 58.0'	76° 06.8'	X	X		
8639348	Money Point, VA	36° 46.7'	76° 18.1'	X	X		
8651370	Duck Pier, NC	36° 11.0'	75° 44.8'	X	X		
NDBC							
41025	Diamond Shoals, NC	35° 00.4'	75° 24.1'		X		
44009	Delaware Bay 26 NM, NJ	38° 27.8'	74° 42.1'		X		
44014	Virginia Beach 64 NM, VA	36° 36.7'	74° 50.2'		X		
TPLM2	Thomas Point, MD	38° 53.9'	76° 26.2'		X		
CHLV2	Chesapeake Light, VA	36° 54.6'	75° 42.6'		X		
CBOS							
mid-Bay	Mid-Bay station, MD	38° 18.0'	76° 12.0'			X(I)	X(I)
VIMS							
GP	Gloucester Point, VA	37° 14.8'	76° 30.0'			X(I)	
ODU							
M3	Chesapeake Bay mouth, VA	36° 57.7'	75° 59.1'			X(F)	X(F)
M5	Chesapeake Bay mouth, VA	37° 00.5'	75° 58.2'			X(F)	X(F)
CBNERR							
	Sweet Hall, VA	37° 34.0'	76° 50.0'				X
	Taskinas Creek, VA	37° 24.0'	76° 42.0'				X
	Claybank, VA	37° 18.0'	76° 33.0'				X
	Goodwin Islands, VA	37° 13.0'	76° 23.0'				X
NOAA COP							
	Newport News, VA	36° 59.3'	76° 26.4'			X(F)	
	Craney Island, VA	36° 53.3'	76° 20.3'			X(F)	

* WL: water level; WD: wind; WV: water velocity; S: salinity; (I): only for Isabel; (F): only for Floyd.

Table 3
Station Information of USGS daily streamflow data in eight tributaries of the Chesapeake Bay recording maximum values during Hurricanes Floyd (1999) and Isabel (2003).

Station ID	River name	Coordinates		Maximum streamflow (CMS)	
		Latitude (N)	Longitude (W)	Floyd	Isabel
01491000	Choptank River	38° 59' 50"	75° 47' 09"	158	36
01578310	Susquehanna River	39° 39' 28"	76° 10' 28"	1476	3380
01594440	Patuxent River	38° 57' 21"	76° 41' 37"	200	139
01646500	Potomac River	38° 56' 59"	77° 07' 40"	403	4225
01668000	Rappahannock River	38° 18' 30"	77° 31' 46"	49	924
01673000	Pamunkey River	37° 46' 03"	77° 19' 57"	168	315
01674500	Mattaponi River	37° 53' 16"	77° 09' 48"	69	104
02037500	James River	37° 33' 47"	77° 32' 50"	352	2324

surface hydrostatic, three-dimensional cross-scale circulation model on unstructured grids (Zhang and Baptista, 2008; Liu et al., 2008a,b; Burla et al., 2010). SELFE uses a semi-implicit Galerkin finite-element method for the pressure gradient and the vertical viscosity terms, which are treated implicitly, and for other terms treated explicitly. To solve the vertical velocity, a finite-volume method is applied to a typical prism, because it serves as a diagnostic variable for local volume conservation when a steep slope is present (Zhang et al., 2004). SELFE treats the advection in the transport equations with the total variation diminishing (TVD) scheme. A higher-order finite-volume TVD scheme is a preferable option in SELFE. TVD is the technique of obtaining high-resolution, second-order, oscillation-free, explicit scalar difference schemes by the addition of a limited anti-diffusive flux to a first-order scheme (Sweby, 1984). Osher (1984) defined the flux differences for a general three-point E-scheme, which is a class of semi-discrete schemes approximating the scalar conservation law. These flux differences are used to define a series of local Courant–Friedrichs–Levy (CFL) numbers. Superbee (Roe, 1986) is used as a flux limiting function. SELFE adapts the Generic Length Scale (GLS) turbulence closure through the General Ocean Turbulence Model (GOTM) suggested by Umlauf and Burchard (2003, 2005), taking advantages from a number of level 2.5 closure schemes such as k–ε (Rodi, 1984), k–ω (Wilcox, 1998); Mellor and Yamada scheme (Mellor and Yamada, 1982). In this study, the k–ε scheme is used.

The horizontal grid used is shown in Fig. 3. This grid has 20,784 elements, 11,582 nodes, and 32,386 sides on the surface. At least three horizontal grid cells resolve the channel of the main Bay. The horizontal spacing of the grid inside the Bay is on average 0.5 km except for the ship channel and the upper part of the tributaries, where the resolution is about 0.1–0.2 km. The triangular unstructured grid with 0.1–0.2 km resolution can cover most of the tidal portion of the major tributaries in the Bay. Transitioning from the Bay to the continental shelf, the resolution became coarser toward the open boundary where the resolution is about 10 km. Although a more refined grid would sufficiently reduce numerical diffusion, computational efficiency should be considered as well, because the time step must be reduced as the grid becomes more refined. In the vertical direction, SELFE uses hybrid-vertical coordinates, which include both terrain-following S-coordinates and Z-coordinates. The terrain-following S layers are placed on top of a series of Z layers. The hybrid vertical coordinate system has the benefits of both S- and Z-coordinates: the S layers used in the shallow region resolve the bottom efficiently and the Z layers, which are only used in the deep region, fend off hydrostatic inconsistency (Zhang and Baptista, 2008). The vertical grid used in the domain has 20 layers in S-coordinates and 10 layers in Z-coordinates. The 20 layers that use S-coordinates cover the entire shallow region down to 43 m in depth, and the 10 layers that use Z-coordinates cover the region from 43–200 m in depth.

3.2. External forcing

3.2.1. Atmospheric forcing

For the hurricane events, the wind and atmospheric pressure fields were generated by the parametric wind model in SLOSH (Jelesnianski et al., 1992). Based on the main hurricane parameters (i.e., hurricane path, atmospheric pressure drop, and radius of maximum wind speed), the model calculates wind speed, wind direction, and air pressure in the pattern of a circularly symmetric, stationary storm. Basically, tangential forces along a surface wind trajectory are balanced by the forces normal to a surface wind trajectory. The formation of wind speed for a stationary, circularly symmetric storm is described as:

$$V(r) = V_M \frac{2(R_M)r}{R_M^2 + r^2} \tag{1}$$

where V_M is the maximum wind speed [m s^{-1}], R_M is the radius of maximum wind speed [m], and r is the distance from the storm center [m]. The moving speed of the storm is estimated by the hourly hurricane track. Typically, the radius of maximum pressure gradient (R_p) does not coincide with the radius of maximum wind speed (Holland, 1980). The ratio is defined as follows:

$$R_p/R_M = [B/(B+1)]^{1/B} \tag{2}$$

where B is the scaling parameter determining the shape of the wind profile. Holland (1980) suggested that B lies between 1 and 2.5 for hurricanes. Detailed applications of this method are found in Shen et al. (2006b) and Wang et al. (2005).

The analytical wind model described above requires three parameters: hurricane path, atmospheric pressure drop, and radius of maximum wind speed. This model is useful during hurricane events, but is not applicable to normal weather conditions. To generate atmospheric forcing with normal weather conditions, an interpolation method is applied by using the data measured at the stations depicted in Fig. 1. The inverse distance weighted (IDW) interpolation method is used for non-hurricane periods. The IDW interpolation is based on the assumption that the interpolating surface should be influenced more by nearby points than by distant points. Shepard's Method is the simplest form of IDW interpolation (Shepard, 1968). The equation used is described as:

$$F(x,y) = \sum_{i=1}^{n} w_i f_i \tag{3}$$

where n is the number of scatter points in the dataset, f_i are the prescribed function values at the scatter points (e.g., the dataset values), and w_i are the weight functions assigned to each scatter point. The weight function used in the method is described as follows (Franke and Nielson, 1980):

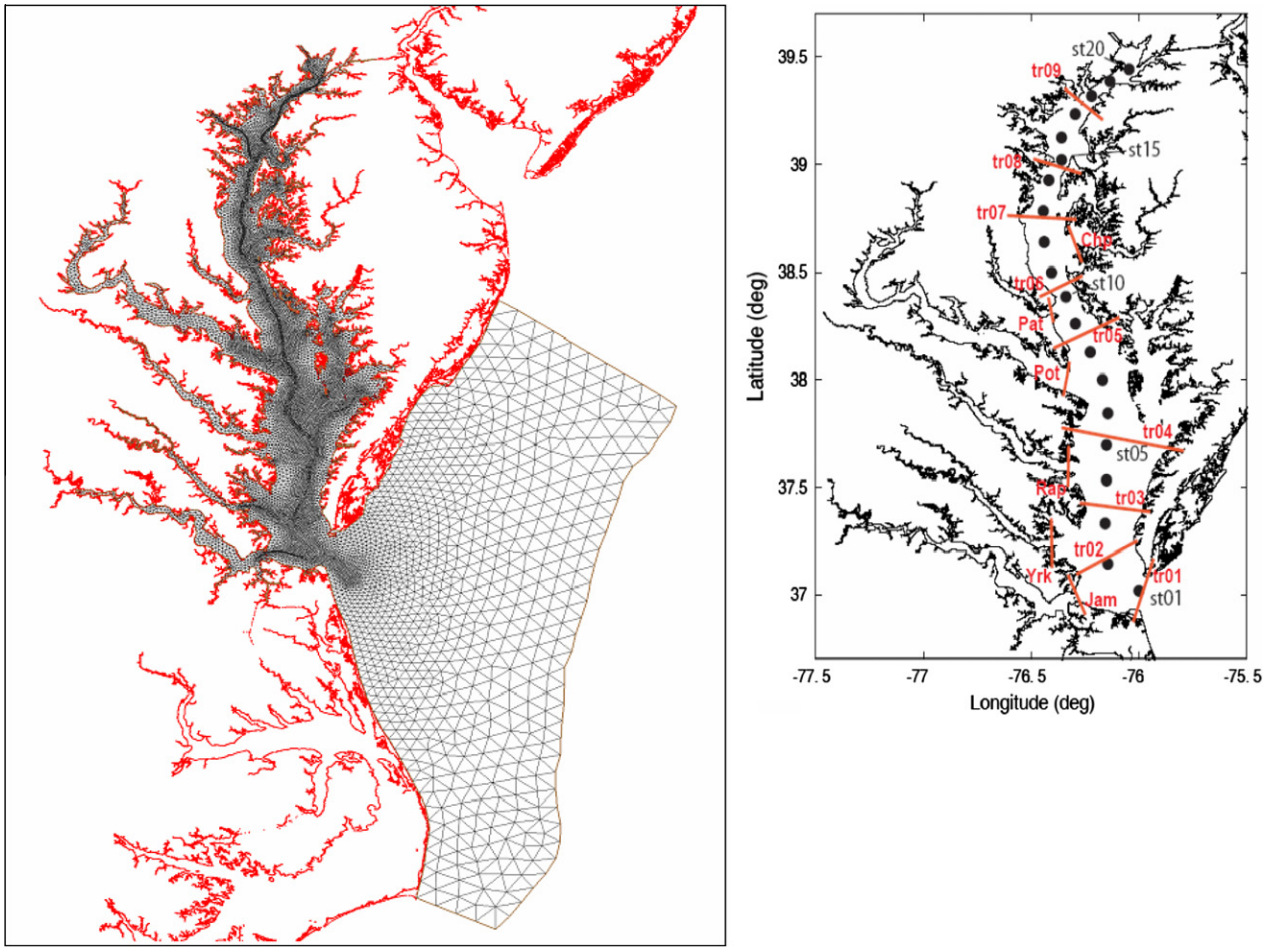

Fig. 3. A horizontal grid for the SELFE model (left) and transects (red lines) and along-channel points (black dots) for transport analysis (right). The grid has 20,784 elements, 11,582 nodes, and 32,386 sides at the surface.

$$w_i = \frac{\left[\frac{R-h_i}{Rh_i}\right]^2}{\sum_{j=1}^{n}\left[\frac{R-h_j}{Rh_j}\right]^2}, \tag{4}$$

where $h_i = \sqrt{(x-x_i)^2 + (y-y_i)^2}$ is the distance from the interpolation point (x,y) to the scatter point (x_i,y_i), R is the distance from the interpolation point to the most distant scatter point, and n is the total number of scatter points.

To correct the parametric wind, the nudging of the observations from the gauge stations in the Bay area including wind speed, direction, and barometric pressure, was used with a modified inverse distance method. Let $F(x,y,t)$ be a variable computed from the parametric wind model at node (x,y). The new variable after correction is $\widehat{F}(x,y,t)$ which can be expressed as:

$$\widehat{F}(x,y,t) = \sum_{i=1}^{N} W_i(x,y)\alpha_i(x,y,t)F(x,y,t)$$

where

$$\alpha_i(x,y,t) = \frac{F_{obs}(x_i,y_i,t)}{F(x_i,y_i,t)}$$

$$W_i(x,y) = \frac{\left[(x-x_i)^2+(y-y_i)^2\right]^{-1}}{\sum_j\left[(x-x_j)^2+(y-y_j)^2\right]^{-1}}$$

$$W_i(x,y) = 1, \quad x = x_i, \quad y = y_i$$

$$W_i(x,y) = 0, \quad x = x_j, \quad y = y_j, \text{ where } i \neq j$$

$\alpha_i(x,y,t)$ is the correction factor for observed variables at the ith station. F_{obs} are the observed variables at the ith station. N is the total number of observation stations. $W_i(x,y)$ is a weighted function corresponding to the ith observation stations. Fig. 4a showed the observed wind and pressure fields at the northern and southern Bay during Hurricanes Floyd and Isabel. Examples of the modeled versus observed wind fields during Hurricane Isabel were shown in Fig. 4b for comparison. Given the relatively dense network of the weather stations in the Chesapeake Bay area, the wind and pressure fields results were successfully used in Shen et al. (2005, 2006a,b).

3.2.2. River inflows

Chesapeake Bay receives freshwater inflow from eight major rivers and from more than 150 creeks (Krome and Corlett, 1990). Since most of these creeks are ungauged and small, we can only account for freshwater measurements from the major rivers. These are the Susquehanna River (at the head of the Bay), the Patuxent, Potomac, Rappahannock, Mattaponi, Pamunkey, and James Rivers on the Western Shore, and the Choptank River on the Eastern Shore. Freshwater inflow records are provided by USGS (http://www.waterdata.usgs.gov/nwis). Daily river inflows varying over time are considered from these eight tributaries of CB, as described in Table 3, with settings of 0 ppt salinity and 15 °C considered constant in time.

3.3. Open boundary conditions

3.3.1. Water elevation

The study area is extended to the 200-m isobath on the continental shelf in the Atlantic Ocean as an alongshore boundary,

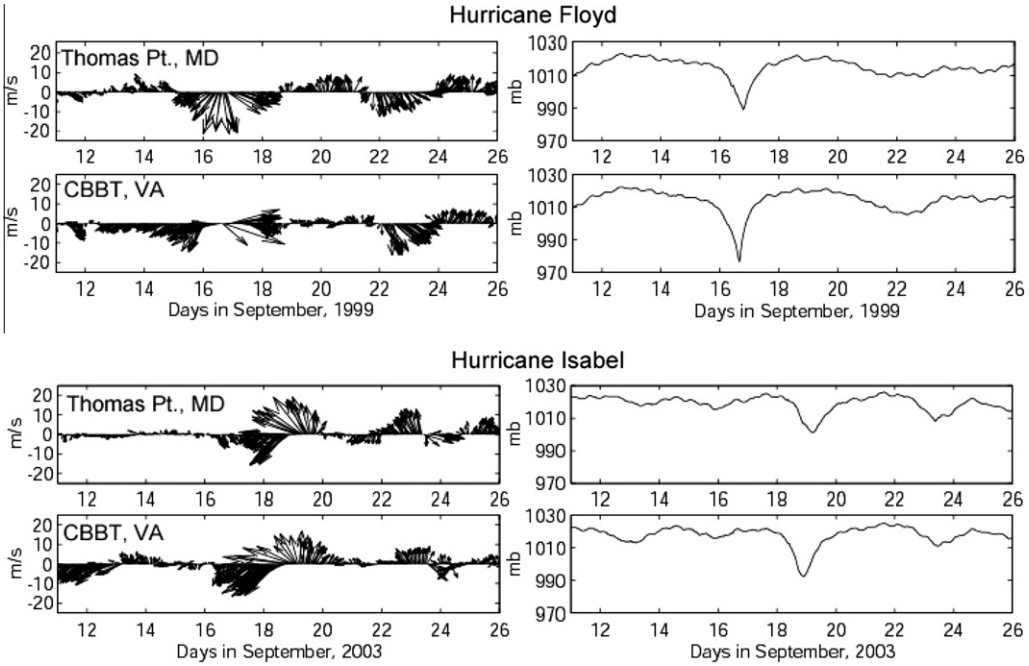

Fig. 4a. Time series plots of wind and pressure data at two stations (from top to bottom: Thomas Point, MD; CBBT, VA) during Hurricane Floyd (upper) and during Hurricane Isabel (lower).

and Ocean City Inlet, MD and Cape Hatteras, NC as northern and southern cross-shore boundaries, respectively. As for the water elevation, two types of boundary conditions are considered to resolve tidal and sub-tidal (primarily induced by meteorological forcing) flows: a Dirichlet-type (clamped) condition (Bills, 1991; Reid, 1990) for the harmonic constants of nine constituents (M_2, S_2, N_2, K_1, O_1, M_4, M_6, K_2, and Q_1), and a Flather-type radiation condition for the sub-tidal component (Flather, 1976; Carter and Merrifield, 2007). An analytical model by Janowitz and Pietrafesa (1996) was used to determine spatial and temporal variations of sub-tidal elevation on the open boundaries during storm events, based on the balance between the production of relative vorticity by bottom Ekman layer pumping and the topographically induced vertical velocity. In this study, the alongshore direction coordinate needs to be transformed from the original due to the consideration of the surge propagation direction and the decision to neglect the bottom friction-induced vertical velocity term from the original form. The results from the analytical model compared well with coastal observations (Cho, 2009).

3.3.2. Salinity and temperature

The Chesapeake Bay Program (CBP) has provided salinity observations in the Bay and its tributaries from 1984 to the present. Salinity is monitored at 49 stations, and sampling occurs once a month during the late fall and winter and twice a month in the warmer months at approximately 1–2 m intervals (CBP, 1993). Outside the Bay, including the continental shelf region, salinity data are provided by the CORIOLIS Data Center (http://www.coriolis.eu.org). Salinity profiles from Argo profilers or oceanographic vessels (XBT, CTD) are collected and controlled in real time by CORIOLIS and analyzed in real time once a week. Salinity fields are obtained on a grid with one-third-degree resolution in latitude and longitude at 57 vertical levels down to 2000 m in the Atlantic Ocean using the objective analysis method (Bretherton et al., 1976). Thus, using the vertical profiles of salinity at all available stations and grid points, initial conditions can be generated at each vertical layer and linearly interpolated in space. The Surface-water Modeling System (SMS) software is incorporated into this interpolation method. Spatially and temporally linearly-interpolated CORIOLIS salinities are imposed as open boundary conditions. Temperature was not explicitly modeled, as salinity dominates the baroclinic effect (Seitz, 1971; Goodrich et al., 1987; Guo and Valle-Levinson, 2008).

4. Model calibration and result

Model-data comparison involves a quantitative evaluation of the performance of the model. The skill assessment we use is based upon computing the mean absolute root-mean-square error (RMSE), the mean absolute relative error (ARE), and R^2, which are defined as:

$$\mathrm{RMSE} = \sqrt{\frac{1}{N}\sum_{i=1}^{N}(P_i - O_i)^2}; \quad ARE = \frac{1}{N}\sum_{i=1}^{N}\left(\left|\frac{P_i - O_i}{O_i}\right|\right) \times 100(\%) \qquad (5)$$

$$R^2 = \frac{\left[n\sum_{i=1}^{n}(P_i \times O_i)\right] - \left[\sum_{i=1}^{n}O_i \times \sum_{i=1}^{n}P_i\right]}{\sqrt{\left\{\left[n\sum_{i=1}^{n}P_i^2\right] - \left[\sum_{i=1}^{n}P_i\right]^2\right\}} \times \sqrt{\left\{\left[n\sum_{i=1}^{n}O_i^2\right] - \left[\sum_{i=1}^{n}O_i\right]^2\right\}}} \qquad (6)$$

where $0 \leqslant ARE \leqslant 100(\%)$, P_i is the model prediction at location (or time) i, and O_i is the corresponding observed value at i. These three skill assessment factors provide an objective and meaningful description of a model's ability to reproduce reliable observations, respectively. Both tidal and sub-tidal values were subjected to the analysis procedures.

4.1. Time series comparison of water level, velocity, and salinity fields

4.1.1. Astronomical tides and storm surges

The model was calibrated with respect to the bottom frictional coefficient by simulating mean tide characteristics. We applied the quadratic stress at the bottom boundary and assumed that the bottom boundary layer is logarithmic with a bottom roughness height

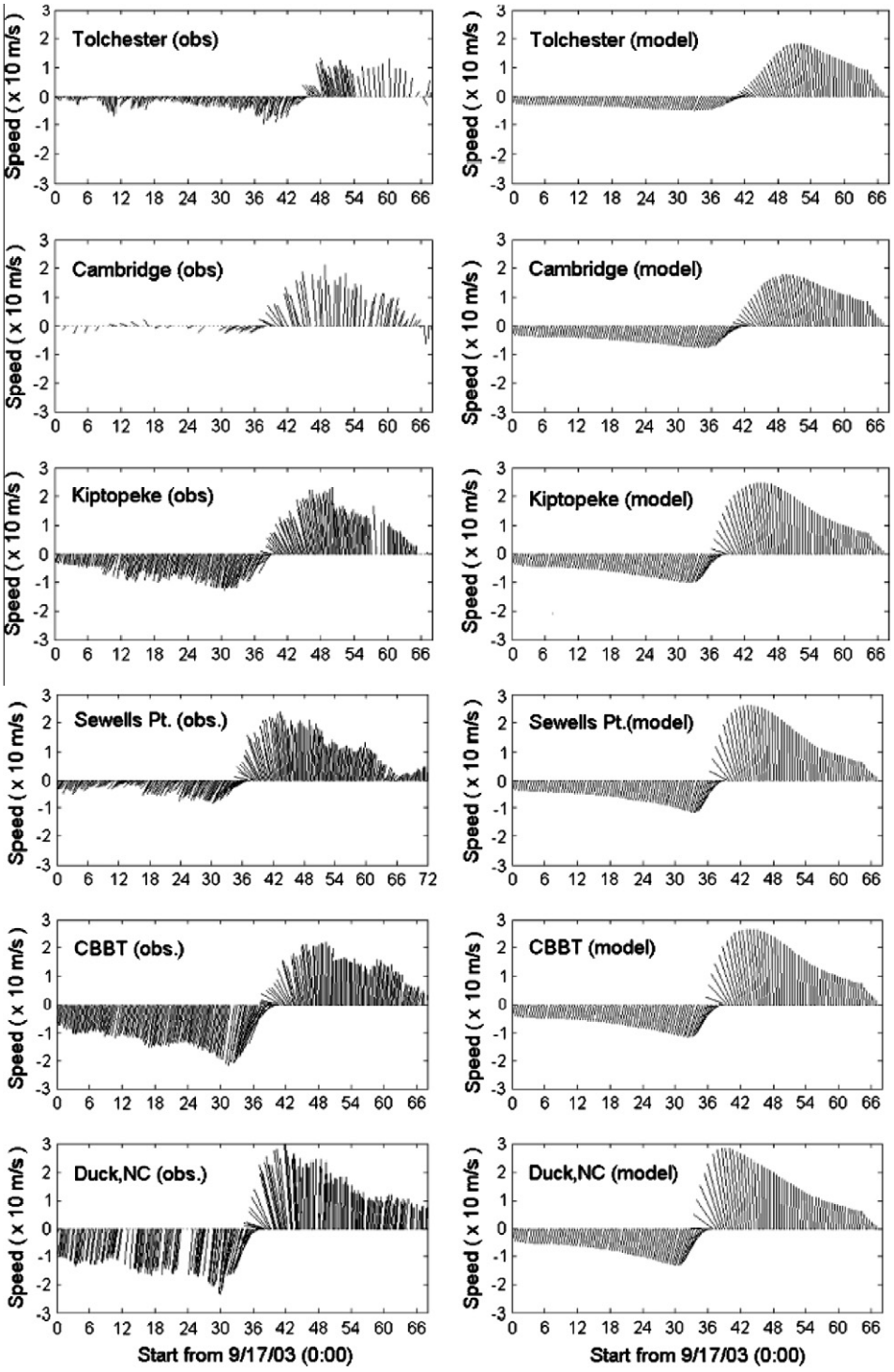

Fig. 4b. The comparison of modeled versus observed wind fields during Hurricane Isabel, observed (left) and modeled (right).

of 0.5 mm. The bottom layer velocity in the 3D baroclinic model was used in conjunction with the logarithmic profile to calculate the bottom stress. The use of calibrated bottom friction parameters during the tidal calculation was found to be adequate to use during hurricane conditions. This is consistent with the reports by Zhong and Li (2006) and Li et al. (2007) in that, by including the vertical stratification in the 3D Chesapeake Bay model, it improved the skill assessment of the calibration and was adequately used for the simulation during the hurricane events.

In order to calibrate the astronomical tides, model results were selected for the last 30 days of the 60-day model run. CB has the tidal characteristics of a reflected, dampened Kelvin wave, with a larger tidal range along the Eastern Shore than the Western Shore (Hicks, 1964; Carter and Pritchard, 1988; Zhong and Li, 2006; Guo and Valle-Levinson, 2007). The mean tidal range decreases from 0.9 m at the Bay's entrance to a minimum of 0.27 m from Plum Point to Annapolis, MD, and then increases to 0.55 m at Havre de Grace, MD, located near the head of the Bay. The model reproduced

these characteristics properly. Harmonic analysis results for four major constituents (M_2, S_2, N_2, and K_1) are shown in Tables 4a and b. The model results have a high correlation and low error compared with observations. The dominant M_2 constituent has an ARE value of 4.1% and a RMSE value of 1.6 cm. To verify the model performance during Hurricanes Floyd and Isabel, model runs were conducted for 15-day periods, from 10–24 September, 1999 and from 12–26 September, 2003, respectively. Time series plots of storm surges at six selected stations during Hurricane Floyd in 1999 and Hurricane Isabel in 2003 are shown in Fig. 5. The model results have high values of R^2 (>0.90) at all of the observation stations, with the exception of the upper Bay station. The RMSE of predicted surges is on the order of 10 cm.

4.1.2. Velocity field

The velocity data were first plotted in a (u, v) diagram to find the major and minor axes for each location, which were then used as a basis to obtain the along-channel velocity component. During hurricane events, the wind-induced sub-tidal velocity superposed on astronomical tidal currents can reach large magnitudes. During Hurricane Floyd, currents were measured exceeding 1 m s^{-1} in the James River, whereas during Hurricane Isabel currents reached 1.5 m s^{-1} at the mid-Bay station. The model-simulated along-channel velocities during Hurricane Floyd were compared with observed velocities at three observation stations: the mid-Bay buoy at depths 2.4 and 10.4 m, Newport News (NN) at 1.7 and 12.7 m, and the M5 station at 3 and 5 m, as shown in Fig. 6(a). The R^2 values all exceed 0.8 and the RMSEs are below 3 cm s^{-1}, except at NN (12.7 m) where the RMSE is 5 cm s^{-1}. During Hurricane Isabel, the comparisons were made at the mid-Bay buoy at 2.4 and 10.4 m and Gloucester Point (GP) at the surface and bottom, as shown in Fig. 6(b). The modeled velocity reproduced the observed velocity at both surface and bottom depths of the mid-Bay station; in particular, a striking feature is apparent at day 19.2, when the peak landward velocity reached a magnitude of 1.5 m s^{-1}. The R^2 values at the mid-Bay buoy both exceeded 0.85. At the GP station, the comparison was not as good, with an R^2 value of about 0.78. Part of the difficulty here is the fact that the major axis of the current is not as well defined, and thus there is some difficulty in defining the axial component of the velocity. Overall, the model results indicate that the SELFE model is capable of reproducing time series of along-channel velocity during both hurricane events in CB mainchannel as well as in its tributaries, the York and James Rivers.

Table 4a
Comparison of observed and predicted mean tidal amplitudes at 11 selected tide gauge stations.

Stations	M2		S2		N2		K1	
	OBS	PRE	OBS	PRE	OBS	PRE	OBS	PRE
(unit: m)								
CBBT	0.38	0.37	0.07	0.09	0.09	0.09	0.06	0.07
Kiptopeke	0.38	0.37	0.07	0.08	0.08	0.08	0.06	0.07
Gloucester point	0.35	0.31	0.07	0.07	0.07	0.07	0.05	0.05
Windmill point	0.17	0.16	0.03	0.04	0.04	0.04	0.03	0.03
Lewisetta	0.18	0.18	0.03	0.04	0.04	0.04	0.02	0.03
Solomon's Island	0.16	0.17	0.02	0.03	0.03	0.04	0.03	0.04
Cambridge	0.23	0.22	0.03	0.04	0.04	0.05	0.05	0.05
Annapolis	0.13	0.12	0.02	0.02	0.03	0.03	0.06	0.06
Baltimore	0.16	0.17	0.02	0.02	0.04	0.04	0.07	0.07
Tolchester beach	0.17	0.19	0.03	0.04	0.04	0.04	0.07	0.07
ARE (%)		4.1		22.6		5.8		11.7
RMSE (m)		0.016		0.010		0.005		0.006

4.1.3. Calculation of volumetric transport

In order to calculate the transport, we followed the formulation used by Kuo and Park (1992):

$$F = \int_A u dA \tag{7a}$$

where u is the velocity normal to each cell area A of a transect. This method can be sufficient to estimate not only longitudinal flows along the main stem, but also lateral volumetric exchanges between the Bay and its tributaries. The time series of the tidally averaged volumetric flux across nine transects along the Chesapeake Bay main stem and six transects in its tributaries was calculated using Eq. (7a) and shown in Fig. 7. During Hurricane Floyd, the net flux in the main Bay and the tributaries are characterized by the following three general patterns: (1) the landward fluxes at all transects were dominant through September 14, (2) the seaward flux became dominant from September 15 to 17, and (3) the landward flux again occurred after September 18 (see Fig. 7a) During Hurricane Isabel, the net flux in the Bay main stem and tributaries are characterized by (1) the landward fluxes across all transects were dominant through September 17, (2) the huge landward flux occurred from the second half on September 18 through the first half on September 19, and (3) the huge return flux again headed seaward from the second half on September 19 to the first half on September 20 and then decreased (Fig. 7b). It is worth noticing that the volume flux during the peak of Hurricane Floyd was dominated by the seaward transport; by contrast, during the peak of Hurricane Isabel, it was dominated by landward transport. The order of magnitude of the surge-induced transport in both events is several times 10^4 m^3/s, which is much larger than the combined river inflow which is on the order of 10^3 m^3/s.

After the events, however, the river discharge began to gather from the watershed and have a significant impact on the re-stratification of the Bay subsequently.

4.1.4. Salinity field

To verify the long-term salinity in SELFE, the modeled salinity data were compared with monthly observed salinity data from CBP. River discharges and open boundary conditions for salinity were specified with the USGS daily stream flow data and the CORIOLIS salinity data. Fig. 8a shows a comparison of surface and bottom salinities at five selected stations (from Duck, North Carolina through the Bay mouth to the upper Bay) for two 150-day periods in 1999 and 2003. SELFE reproduced the temporal salinity variation with a good agreement in the vertical stratification. The model highlighted the decrease in surface salinity induced by high freshwater inflows at the end of January 1999 and at the end of March 2003. Fig. 8b showed the skill metrics of the comparison. Overall, the score was high with the root-mean-square error around 2–3 ppt for both surface and bottom salinities indicating that the SELFE model is capable of simulating the baroclinic process and the underlying salinity structure. Fig. 9 shows additional comparisons made during Hurricane Floyd, whereby the model and measured salinity time series were compared at the mid-depth and bottom of the M5 Station and the surface of the M3 Station. Again, the model performed well in catching the major salinity drawdown during 17–18 September, when the major sub-tidal velocity turned seaward. The model also reproduced the rebound of salinity after the event. We low-pass filtered the sub-tidal variation of the modeled and observed values, and then made the comparison. The metrics for the skill showed a better prediction at mid- and bottom depths at Station M5 ($R^2 \sim 0.65$) than that on the surface of Station M3 ($R^2 \sim 0.45$). We believe the error is introduced due to the uncertainty on the amount of the rainfall that fell directly onto the surface of the Bay water and its subsequent effects.

Table 4b
Comparison of observed and predicted mean tidal phases at 11 selected tide gauge stations.

Stations	M2		S2		N2		K1	
	OBS	PRE	OBS	PRE	OBS	PRE	OBS	PRE
(unit: m)								
CBBT	235.3	235.3	255.9	255.9	218.1	218.1	109.1	109.1
Kiptopeke	247.9	251.7	270.8	271.7	229.2	234.6	119.3	120.5
Gloucester point	268.3	267.0	288.7	287.8	250.9	249.2	125.6	125.7
Windmill point	317.3	326.6	334.0	344.7	297.2	309.8	148.7	159.4
Lewisetta	33.8	30.6	54.7	54.3	7.6	11.1	205.0	210.8
Solomon's Island	54.2	47.9	70.5	74.3	32.4	27.8	243.7	238.4
Cambridge	114.7	91.6	139.0	120.2	94.0	72.1	269.4	252.2
Annapolis	147.2	133.1	175.0	157.7	126.0	115.0	283.3	272.2
Baltimore	193.9	191.2	213.4	216.8	173.4	170.5	296.6	281.5
Tolchester beach	202.7	194.4	227.4	222.0	176.0	173.0	287.9	277.5
ARE (%)		6.1		3.7		10.3		3.2
RMSE (deg)		9.8		9.1		9.2		9.7

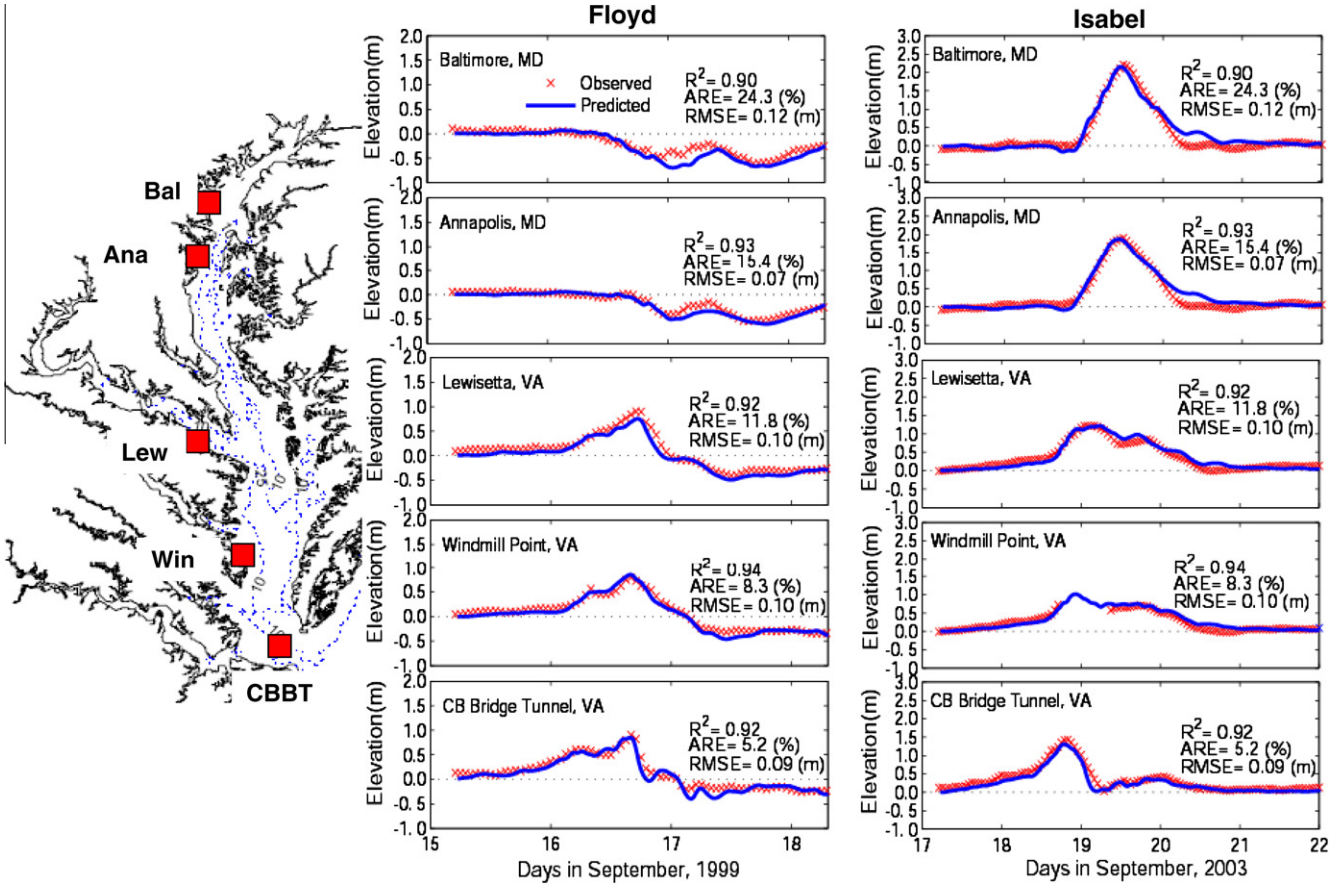

Fig. 5. Surge height comparison between observed (red) and predicted (blue) at five selected stations during Hurricanes Floyd (left) and Isabel (right).

4.2. Spatial pattern of water level, salinity, and velocity fields

4.2.1. Horizontal distribution of elevation and depth-averaged flow

The time sequences of elevation and sub-tidal depth-integrated flows during Hurricane Floyd were shown in Fig. 10. The left panel was coincided with the hurricane approaching phase and the right panel with the phase of the land-falling and resurgence. The background color denotes the water elevation and the depth-averaged flow is the low-pass filtered sub-tidal velocity (using the Lanczos filter for removing the intratidal component). On 16 September at 09:00 UTC, a northeasterly wind of 10.9 m s^{-1} began to drive the water from the continental shelf into the Bay, and consequently generated the first stage peak of storm surge in the lower Bay, as shown in Fig. 10(b). Northeasterly and easterly winds continued to blow up to 16:00 and 17:00 UTC (Fig. 10(d) and (e)) when the water from both the northern Bay and the continental shelf converged making the surge elevation reach to its maximum. Directly after 17:00 UTC on the same day, as the eye of the hurricane swept over the Bay mouth, the winds changed to a northwesterly direction with a maximum speed of 23.4 m s^{-1} (not shown), which elevated the water level specifically along the Eastern Shore of Virginia. From 18:00 UTC on, consistent large outflows from the Bay to the ocean were observed and the surge height started to decrease, as shown in Fig. 10(f), (g), and (h). For Hurricane Isabel, time sequences of the elevation and sub-tidal depth-integrated flows were plotted in Fig. 11. (It should be noted that different

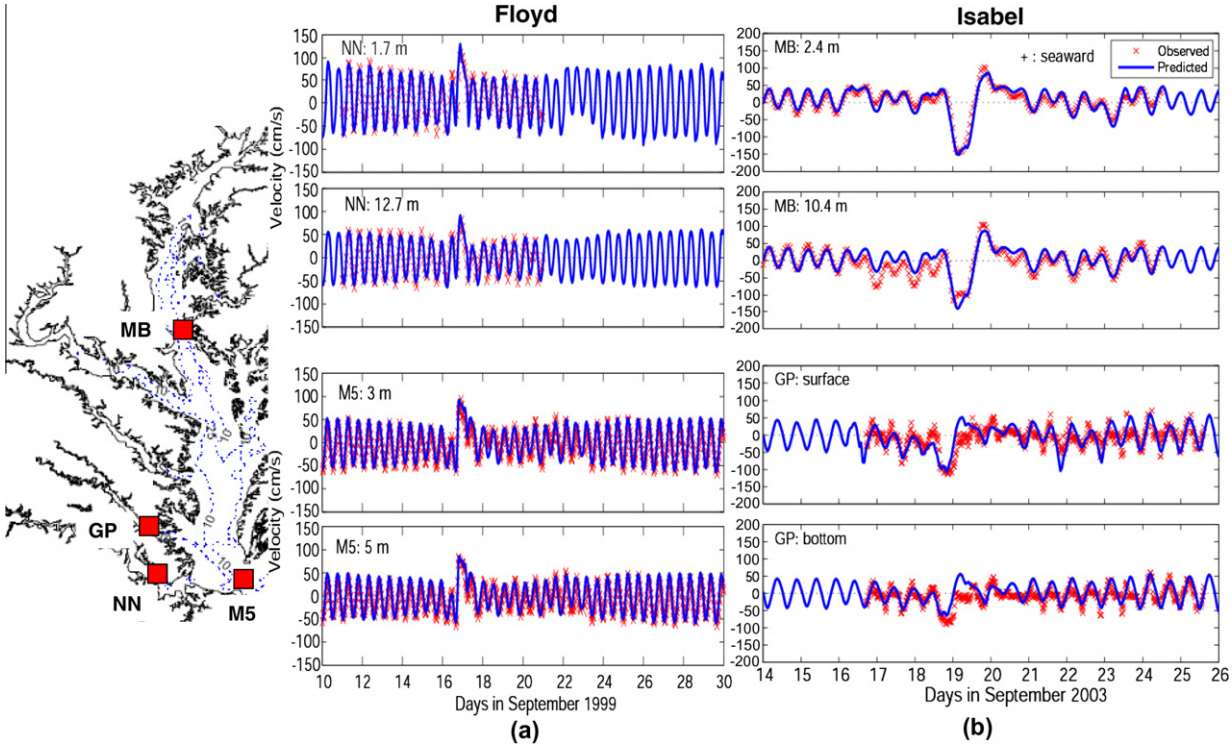

Fig. 6. Comparison of observed and predicted along-channel velocity during Hurricane Floyd in (a) and during Hurricane Isabel in (b).

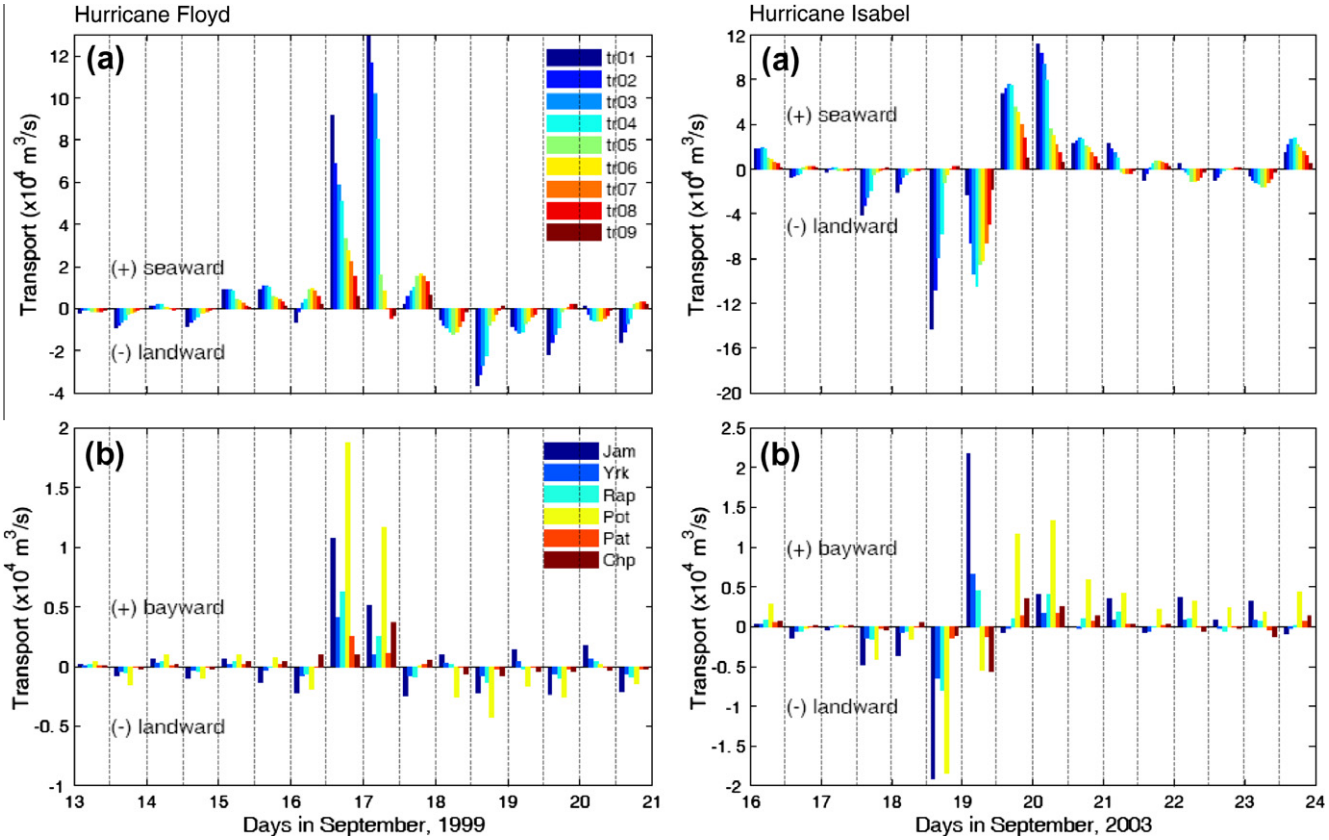

Fig. 7. Tidally averaged mean volumetric transport represented at half-day intervals at transects in the main stem Bay (top) and the tributaries (bottom) for the Hurricane Floyd (left) and Hurricane Isabel (right).

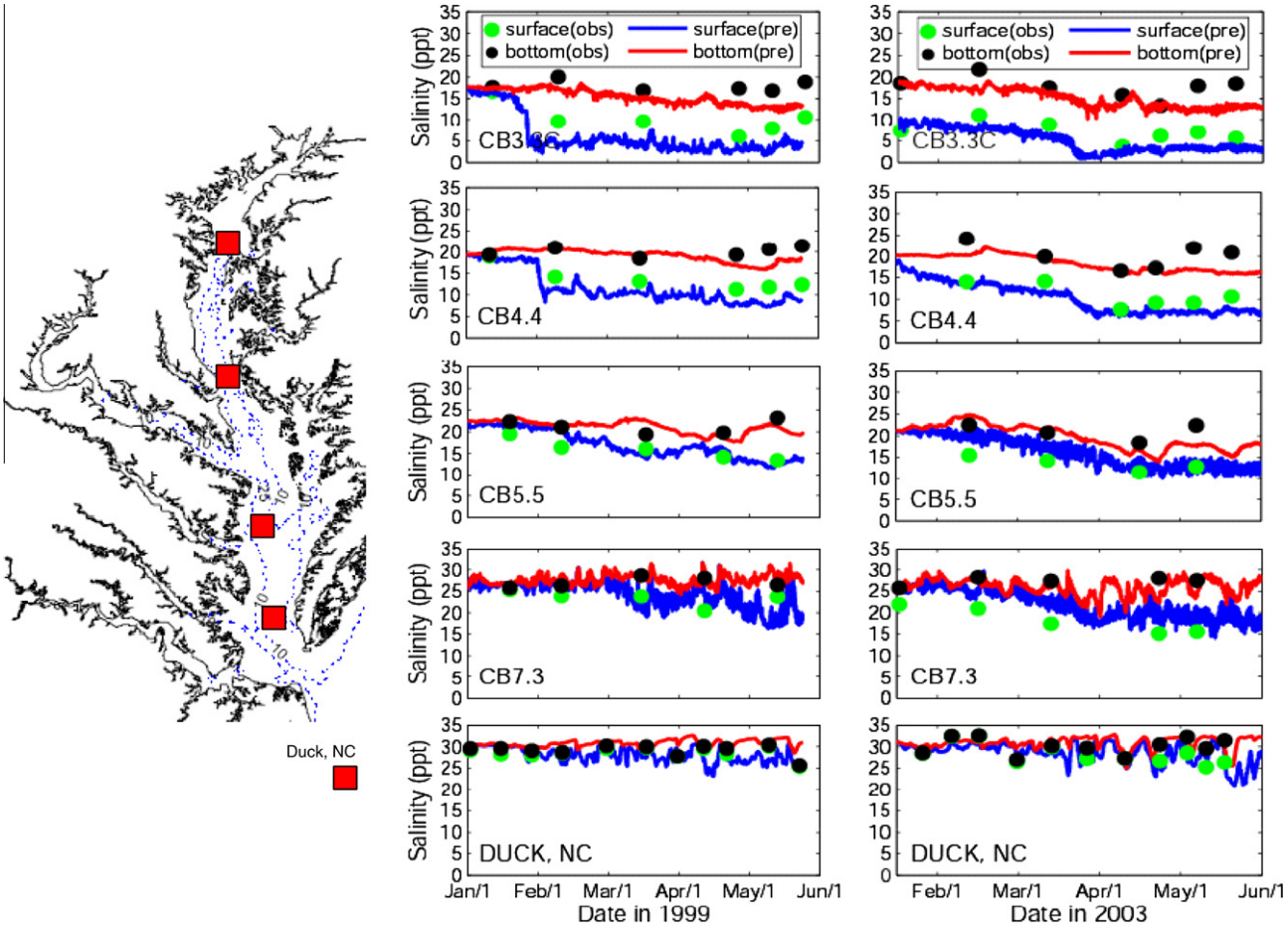

Fig. 8a. Comparison of observed and predicted salinity (surface and bottom) at five selected stations for spring 1999 (left) and spring 2003 (right). Model results (red: bottom; blue: surface) and observed data (black circle: bottom; green circle: surface).

background color scales was used for Figs. 10 and 11). There were initially a seaward outflow driven by northeasterly winds (Fig. 11(a)), but from 15:00 UTC, 18 September, the seaward outflow along the Bay mouth started to decrease and changed to an inflow. As the remote northeasterly and easterly winds strengthened up to 23 m/s during the period from 15:00 to 21:00 UTC, September 18, it generated very strong landward inflows from the continental shelf into the Bay as shown in Fig. 11(c) and (d). Over the period from 01:00 UTC to 03:00 UTC on 19 September, as Hurricane Isabel made the landfall and moved inland on a northwest track, the trailing edge of the cyclonic, local winds (i.e., southeasterly and southerly winds) became dominant. This pattern of wind is very persistent and efficient in intensifying the northward inflows and set up against the head of the upper Bay (Fig. 11(d), (e), and (f)). During this period, the peak surge height gradually built up in the upper Bay (not shown). In the end, the pressure gradient created by the sea level slope from the north to the south drove the water in an opposite direction to that of the wind, as shown in Fig. 11(h). From the comparison of the Bay's water level response to hurricanes, it was found that the storm surge in the Bay has two distinct stages: an initial stage setup by the remote winds and the second stage induced by the local winds. For the initial stage, the remote wind was setup by both hurricanes initiated in the coastal ocean resulting in the similar influx of storm surge; but for the second surge, the responses of the Bay to the two hurricanes were significantly different. Hurricane Floyd was followed by down-Bay winds that canceled the initial setup and caused a set-down from the upper Bay. Hurricane Isabel, on the other hand, was followed by up-Bay winds, which reinforced the initial setup and continued to increase the water level against the head of the Bay.

4.2.2. Along-channel variation of velocity and salinity fields

Longitudinal distributions of 25-h tidally averaged velocity and salinity during the hurricanes are plotted in Fig. 12(a) and (b) for Hurricanes Floyd and Isabel, respectively. During Hurricane Floyd, on 16 September, the Bay had a two-layered circulation prior to the passage of the eye of the storm, in which fresher water flowed seaward whereas saltwater flowed landward. After the eye had passed over the mouth of the Bay (17 September), the flow direction changed to seaward along the entire cross-section in the lower Bay and mainly two-layered circulation in the deep portion of the Bay. The salinity decreased by approximately 3–4 ppt. On the next day (18 September), a landward return flow occurred throughout the entire transect (Fig. 12(a)). Stratification in the deep channel was increased by 3–4 ppt due to a relatively strong saltier water inflow through the bottom layer. Within a week, the non-tidal flow across the cross-section appeared to return to a two-layered circulation pattern, and the vertical salinity structure appeared to be adjusted by the restratification process (not shown).

During Hurricane Isabel, prior to the passage of the strongest wind, the salinity difference between surface and bottom waters in the deep channel was approximately 6–7 ppt, which is 4–5 ppt greater than the pre-Floyd condition. On 18 September, with the northeasterly wind on the continental shelf, we see that vertically homogeneous saltwater was pumping into the Bay from the ocean (Fig. 12(b)). The mid- and upper Bay portions also have strong

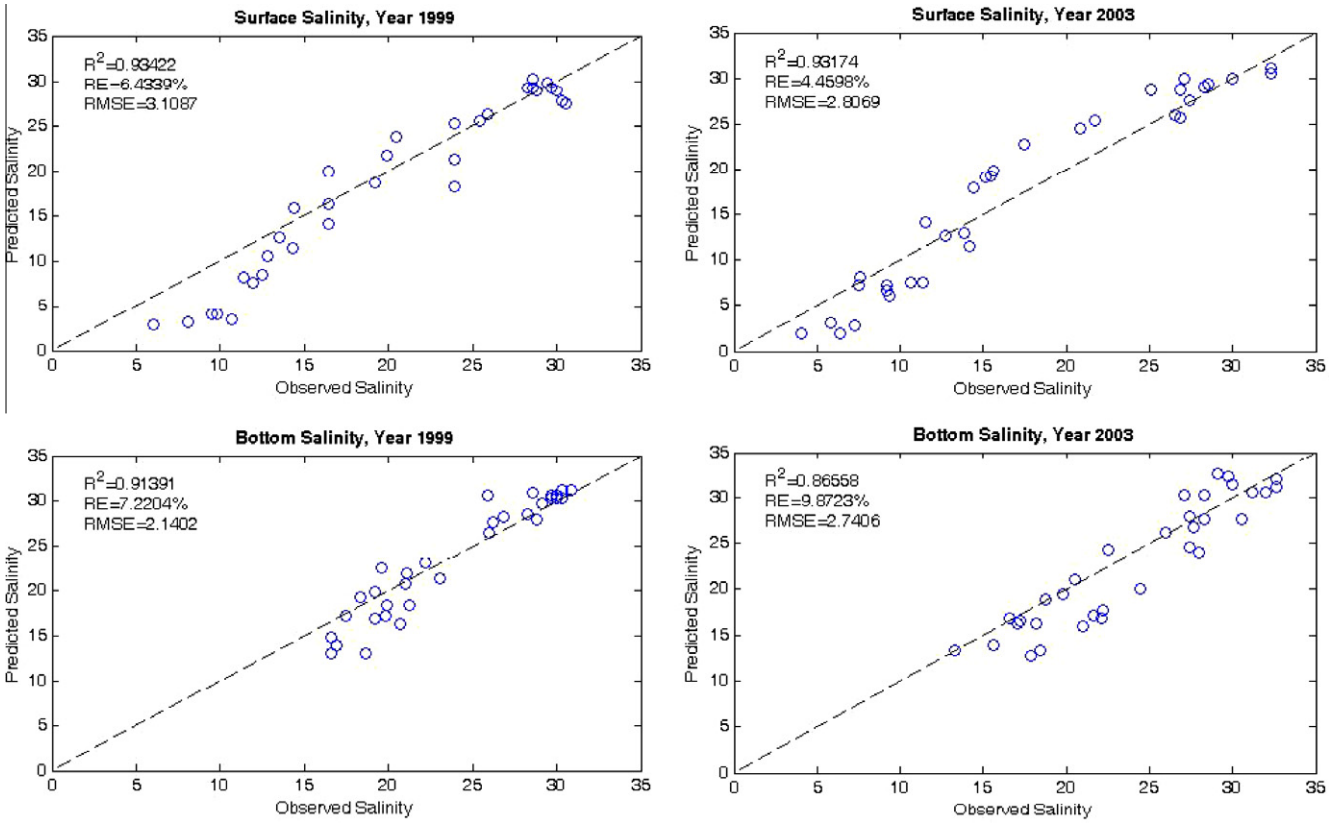

Fig. 8b. The statistical comparison of the modeled versus observed surface and bottom salinity shown in Fig. 8a.

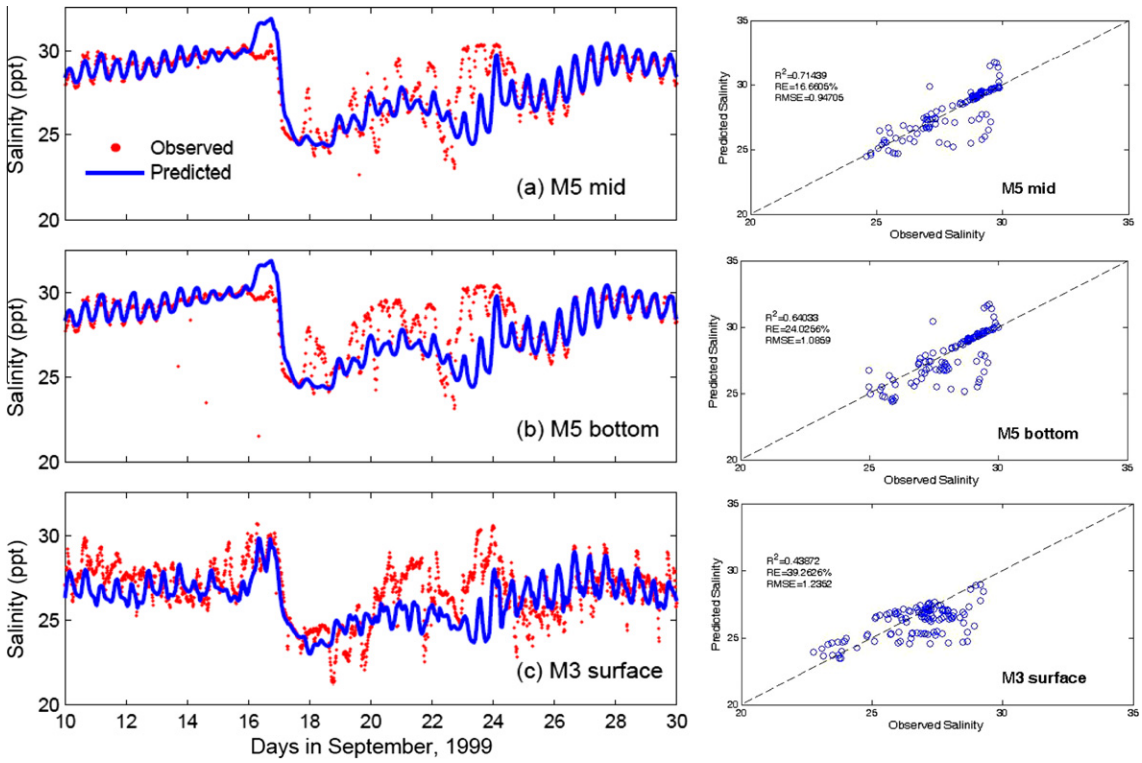

Fig. 9. Salinity comparison between observation data (red) and model prediction during Hurricane Floyd: (a) mid depth at M5, (b) near bottom at M5, and (c) near surface at M3 (left) and related statistical comparison (right).

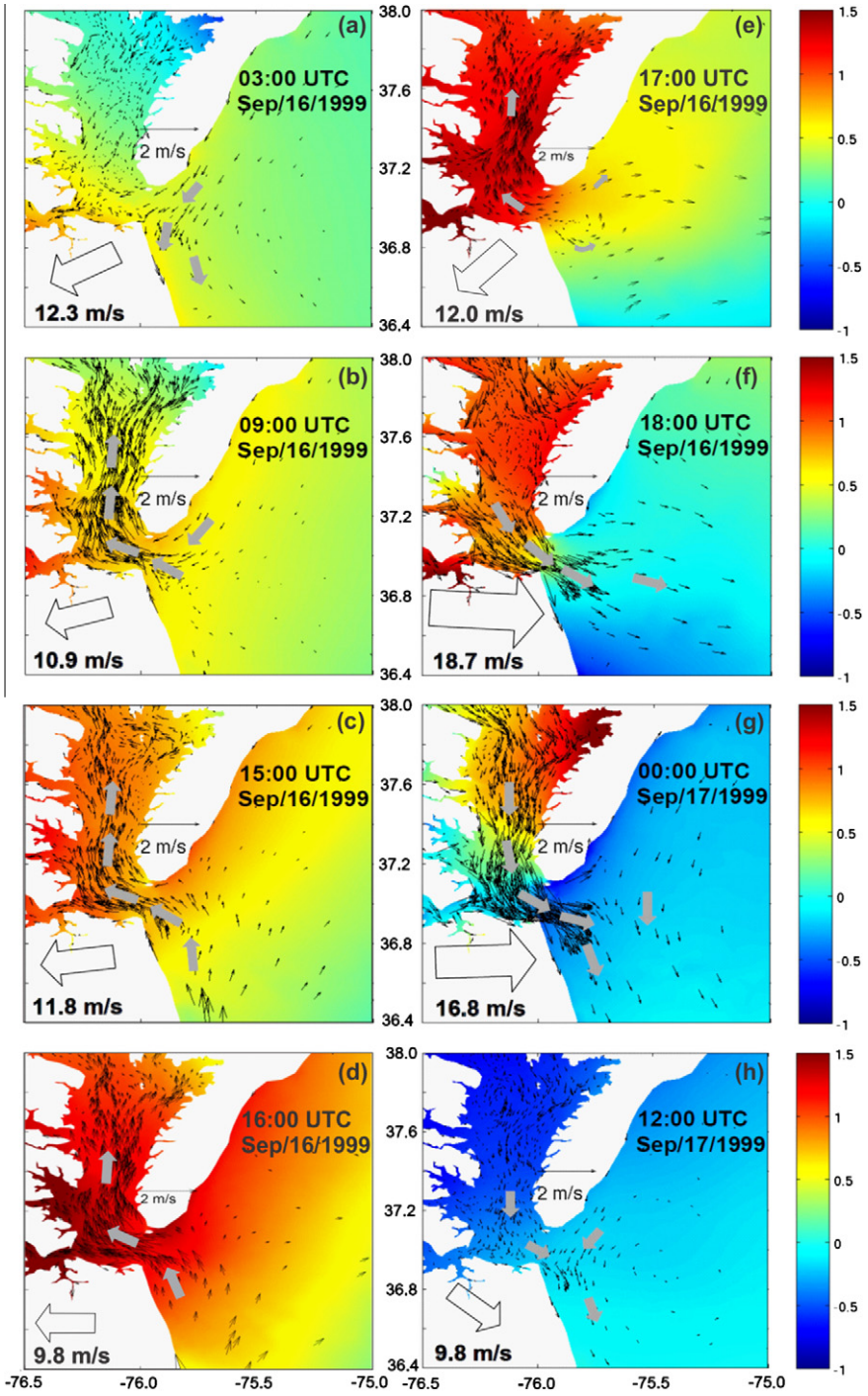

Fig. 10. Horizontal distributions of depth-integrated flow (thin arrows) at the southern portion of the Chesapeake Bay during Hurricane Floyd with time sequence from (a) September 16 03:00 UTC to (h) September 17 12:00 UTC. Colored map represents storm height, the thick open arrow specifies wind speed and direction recorded at CBBT, VA, and the gray arrow is the general direction of the flow.

components of landward bottom flow. On 19 September, when the hurricane passed by, a strong band of surface landward flow showed in the mid- and upper Bay portions and the previously stratified water became relatively well-mixed. On 20 September, the very strong seaward flow rebounded, and the stratification in the vertical water column of the Bay started to increase by 2, 1.5, and 5 ppt in the upper, middle, and the lower Bay, respectively (Fig. 12(b)). Within about a week, the net flow appears to return to a two-layered circulation pattern with a 7–8 ppt salinity difference between surface and bottom waters in the channel (not shown).

A comparison of the Bay's response to the two hurricanes features a few highlights: (1) Prior to the storms, there was a significant difference between the observed stratification (ΔS) in the Bay (Table 5). At CB4.4, pre-Floyd stratification was nearly 4 ppt whereas pre-Isabel stratification was nearly 11.5 ppt. (2) In the lower Bay, it is clear that the saltwater intrusion occurred during both hurricanes. (3) Overall, the winds during both hurricanes generated vertical mixing that destratified the water column. Even during the peak of the hurricane events, however, the deep portion of the mid-Bay remained stratified.

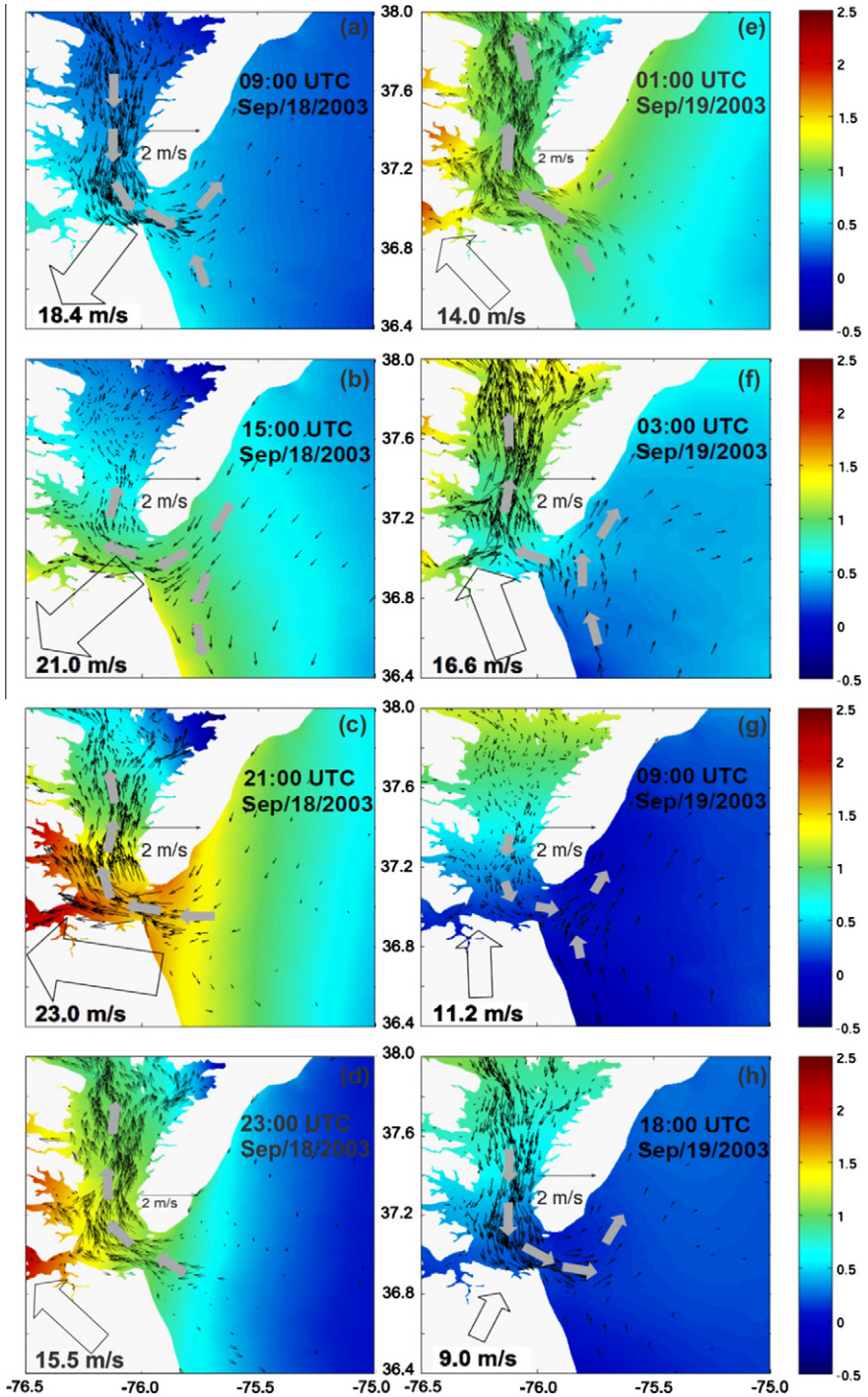

Fig. 11. Horizontal distributions of depth-integrated flow (thin arrows) at the southern portion of the Chesapeake Bay during Hurricane Isabel with time sequence from (a) September 18 09:00 UTC to (h) September 19 18:00 UTC. All legends are the same as depicted in Fig. 10 except the scale of the colored bar is slightly different.

4.3. Cross-sectional salt flux

Following Lerczak et al. (2006), the total salt flux is expressed by:

$$F_s = \left\langle \iint usdA \right\rangle \tag{7b}$$

where the angle bracket denotes a 33-h low-pass filter, u is the axial velocity, s is salinity, and the cross-sectional integral within the angle bracket represents the instantaneous salt flux. F_s can further be decomposed as:

$$\begin{aligned} F_s &= \langle \iint (u_0 + u_E + u_T)(S_0 + S_E + S_T)dA \rangle \\ &\approx \langle \iint (u_0 S_0 + u_E S_E + u_T S_T)dA \rangle \\ &= Q_f S_0 + F_E + F_T \end{aligned} \tag{8}$$

in which u and S are decamped into tidally and cross-sectionally averaged (u_0 and S_0), tidally averaged and cross-sectionally varying (u_E and S_E), and tidally and cross-sectionally varying (u_T and S_T) components. Here u_0 is defined as the low-passed volume transport divided by the low-passed cross-sectional area. Thus, Q_f includes the volume transport resulting from the correlation between tidal currents and fluctuation in the cross-sectional area, and S_0 is the

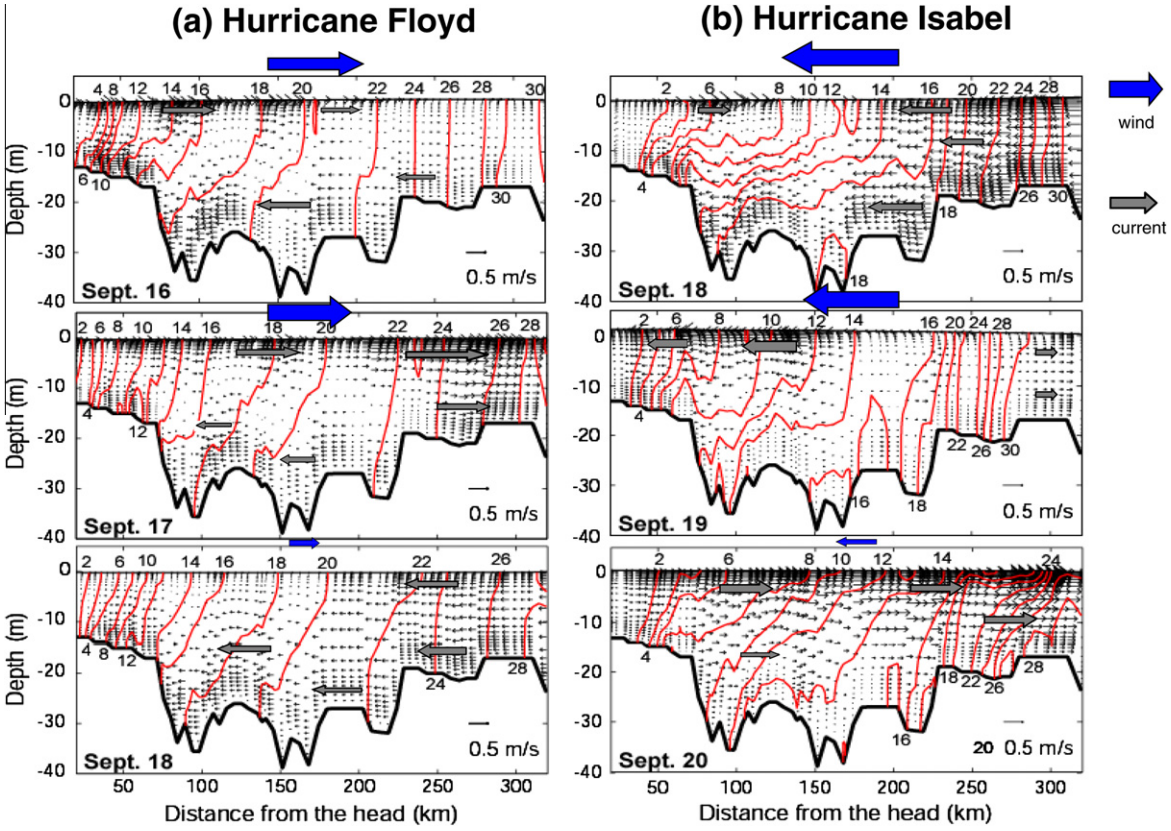

Fig. 12. Longitudinal distributions of tidally averaged (25 h) velocity and salinity in the along-channel section of the Chesapeake Bay for three days during Hurricanes Floyd (left) and Isabel (right).

Table 5
Comparison of observed stratification between pre-storm and post-storm at four selected CBP stations during Hurricanes Floyd (1999) and Isabel (2003).

Station ID	Salinity Stratification (ppt)			
	Floyd (1999)		Isabel (2003)	
	pre-storm (Aug/17–18)	post-storm (Sep/21–22)	pre-storm (Sep/15–16)	post-storm (Sep/22–23)
CB3.1	2.43	7.80	9.03	2.39
CB3.2	1.77	6.72	8.37	1.75
CB4.4	4.10	4.85	11.52	4.97
CB5.3	3.04	5.45	10.90	8.61

tidally and cross-sectionally averaged salinity. The resulting three terms are the salt fluxes due to sub-tidal cross-sectionally averaged transport ($Q_f S_0$), the sub-tidal shear dispersion (F_E), and tidal oscillations (F_T). As pointed out by Lerczak et al. (2006), in the absence of axial wind, the two up-estuary salt fluxes (F_E and F_T) balance the down-estuary salt loss to river discharge ($Q_f S_0$).

4.3.1. Longitudinal distribution

The instantaneous total flux and the tidally averaged total salt flux F_s were generated at nine cross-sections in CB for Hurricanes Floyd (Fig. 13, upper panel) and Isabel (Fig. 13, lower panel). In Fig. 13(a), before the hurricanes make landfall, it is obvious that the ocean saltwater influx was induced by the remote northeasterly wind of both hurricanes. The magnitude of the flux at the Bay mouth due to Isabel appears to be greater than that due to Floyd. This can be attributed to the rotation of the unsteady winds from the northeasterly to easterly, which favored Isabel. For Hurricane Floyd, the initial salt influx only reaches the lower Bay, whereas during Isabel the salt flux effects were felt at the northern end of the Middle Bay. The strong seaward flow induced by down-Bay winds during Floyd restricted landward salt flux to the upper Bay, whereas landward flow enhanced by up-Bay winds during Hurricane Isabel strengthened the landward salt flux to the upper Bay. In the subsequent time sequence, shown in Fig. 13(b)–(e), the flux is affected by the local wind and dominated by the large pulse of volume transport in F_s. Most of the time, the direction of salt transport is unidirectional across the nine transects of the Bay, with the exceptions of (c) for Floyd and (e) for Isabel. The salt is either flushed out (Floyd) or pumped in (Isabel) to the Bay as a result of the net volume transport, and F_s is dominated by $Q_f S_0$ rather than F_E or F_T.

4.3.2. Oceanic salt influx

Further details of the oceanic salt influx at the Bay mouth are shown in Fig. 14, in which the time series of instantaneous total salt flux F_s are shown on the top panel for Hurricanes Floyd (left) and Isabel (right). The full tidal cycle of 16 September, 1999 and two tidal cycles of 17–18 September, 2003, which were before the hurricanes made landfall, are marked by the dark shaded area. The lateral distribution of the total cross-sectional tidally averaged

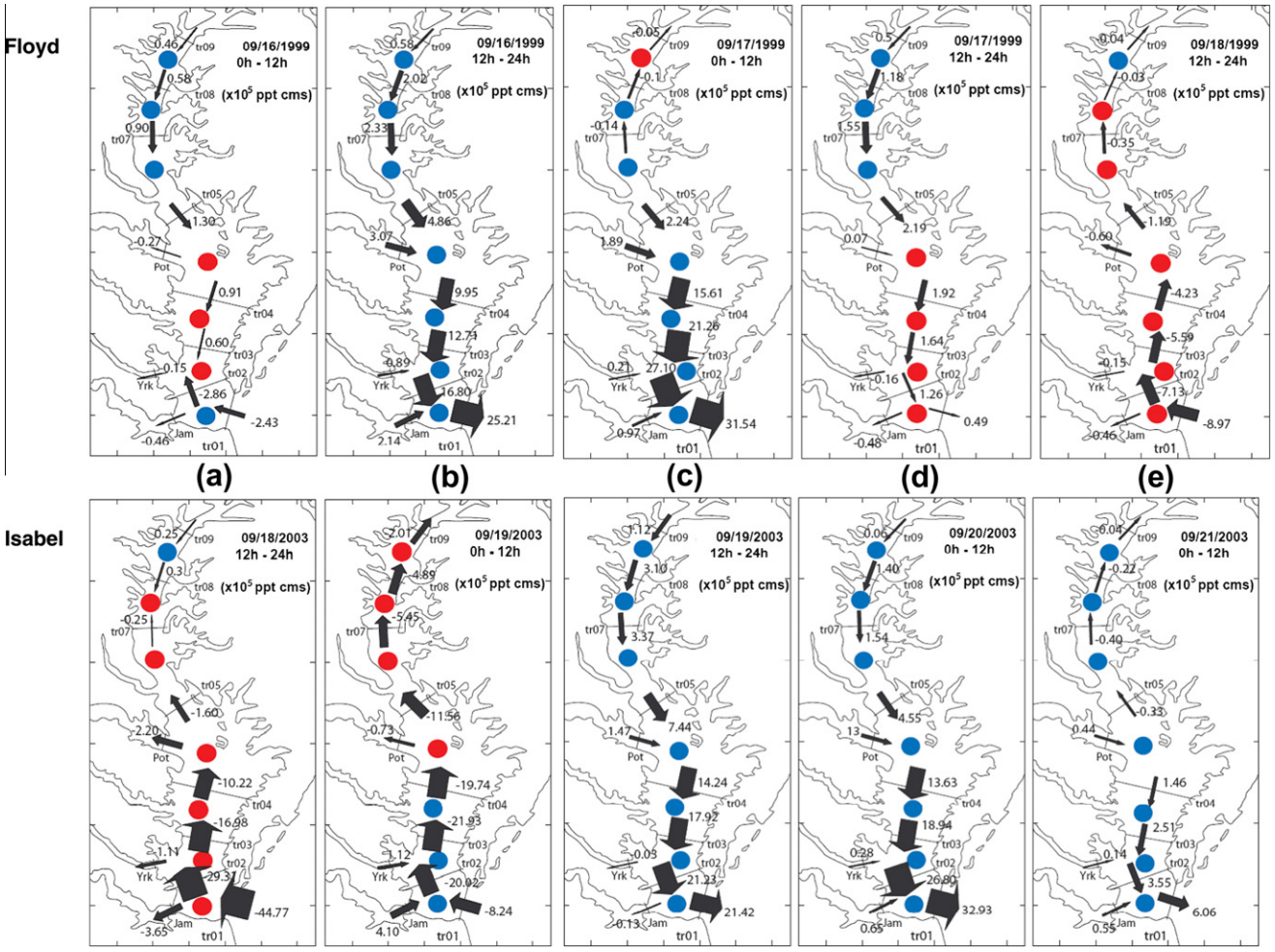

Fig. 13. Time sequence of net salt flux averaged over a tidal cycle at transects in Chesapeake Bay during Hurricanes Floyd (top) and Isabel (bottom). The positive value denotes seaward flux and red and blue colors represent the increase and decrease of salt, respectively.

salt flux over the period is shown in the middle panel. It is clear that the tidally averaged salt flux was negative, indicating an oceanic saltwater influx from the continental shelf into the Bay for both hurricanes. The salt influxes were concentrated in the deep portion of the channels at 0–6 km and 14.8–15.2 km, rather than in the shoal region at the Cape Henry cross-section. The baroclinic component of the tidally averaged salt flux excluding $Q_f S_0$ was also calculated, and the magnitude is about half of the total flux, as shown in the bottom panel. It is concluded that both barotropic and baroclinic components contributed to oceanic saltwater influxes during the first stages of the hurricanes.

5. Analysis of the local axial wind-induced mixing process—a controlled experiment

Local winds that exert stress on the surface of the water can cause direct wind mixing, and reduce the stratification, but a moderate down-estuary wind can also induce a wind-straining effect, which under certain conditions increases stratification (Scully et al., 2005). Due to their tracks, Hurricanes Floyd and Isabel produced distinctly different local wind stresses, a down-estuary and an up-estuary stress. This difference provides a natural test bed for examining how the direction of the axial wind affects the vertical stratification and the salt transport.

In order to reasonably compare the wind-induced mixing process between the two hurricanes, a controlled experiment is required to ensure that the local and remote winds are separated, that different pre- and post-hurricane conditions are equalized, and that the background conditions are uniform. To start with, the background state of the estuarine system is required to be in a quasi-steady state prior to the hurricane. Upon the passage of the hurricane, the estuarine system will experience the hurricane's wind forcing, and then eventually return to the quasi-steady state when all of the external perturbations are removed. Table 6 shows seven experiments that were performed to examine the mixing process induced by the local and remote meteorological external forcing during the two hurricanes, Floyd (FL) and Isabel (IS). Four types of wind forcing were considered: no wind (NW), local (L), remote (R), and combined (C). Fig. 15 shows wind and pressure fields selected from the real hurricane conditions for the controlled experiment. The base run used only the M_2 tidal constituent and a constant river discharge of 550 $m^3\ s^{-1}$, which characterizes the summer average flow in the Bay. The use of a single semi-diurnal tidal constituent precludes investigation of the effect of spring–neap tides on salinity. A constant ambient current of 10 $cm\ s^{-1}$ was specified at the cross-shore open boundaries in the continental shelf, based on the work of Cho (2009). To obtain the initial salinity condition in an equilibrium state, the model was spun up for 180 days without meteorological forcing from a cold start, such that salinity had a linear variation horizontally from the Bay head (0 ppt) to the open ocean (34–35 ppt) with no stratification in the vertical direction. When the relative gradient of tidally averaged

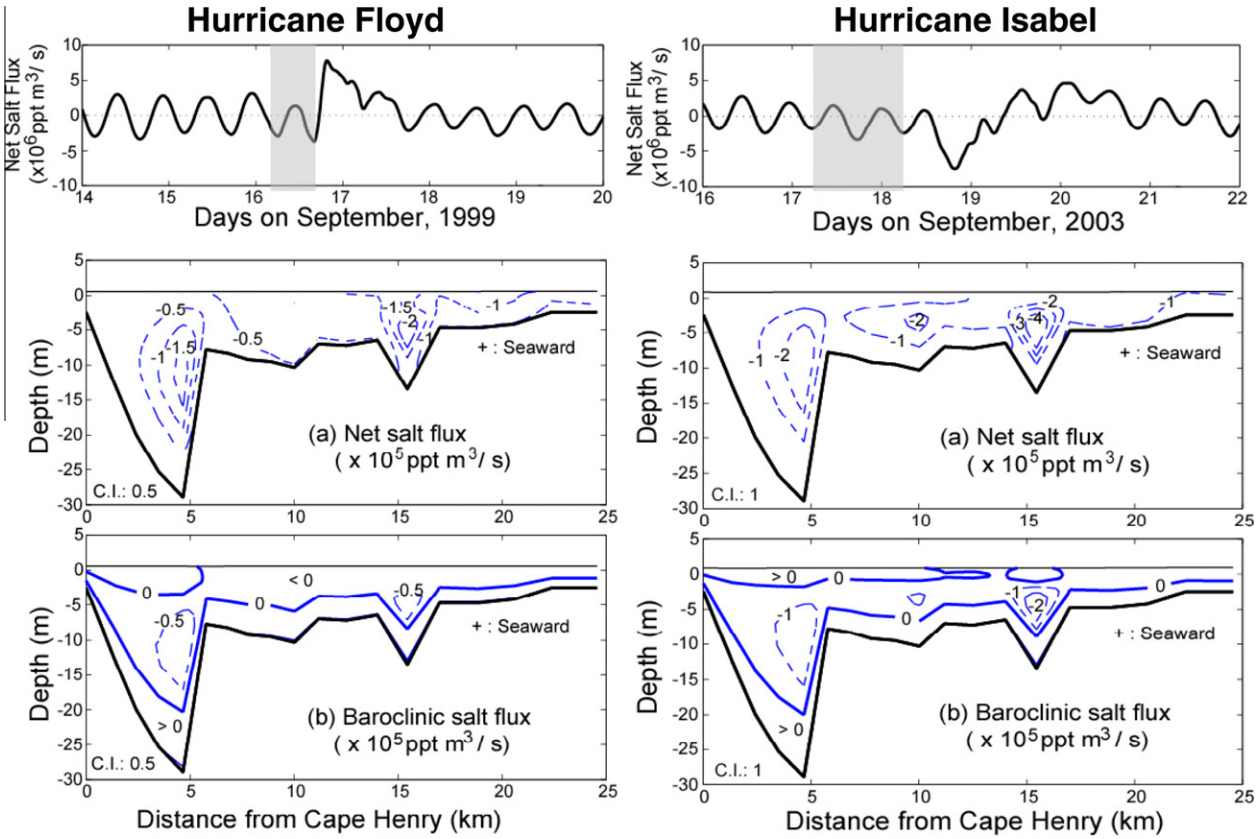

Fig. 14. Estimated net salt flux and baroclinic salt flux at tr01 during Hurricanes Floyd (left) and Isabel (right). The fluxes were averaged over the period shaded.

Table 6
Summary of numerical experiments performed.

Experiments	Winds	Total river discharge ($m^3\ s^{-1}$)	Ambient current ($cm\ s^{-1}$)	Subtidal alongshore PG*
NW	No wind	550	10	
FL-C	Combined winds (Floyd)	550	10	O
IS-C	Combined winds (Isabel)	550	10	O
FL-L	Local winds (Floyd)	550	10	
IS-L	Local winds (Isabel)	550	10	
FL-R	Remote winds (Floyd)	550	10	O
IS-R	Remote winds (Isabel)	550	10	O

* PG represents the pressure gradient.

salinity difference with respect to time is reduced to an insignificantly small value (0.1%), it is assumed that the salinity has reached the equilibrium state. The modeled salinity reached the equilibrium state approximately 150 days after the cold start.

5.1. Response of instantaneous velocity and salinity to the local wind

We first examined the time series of longitudinal velocities (surface and bottom) under local wind forcing, as shown in Fig. 16. The time series were plotted for five stations: CB3.3C, in the upper Bay, CB4.4 and CB5.3 in the middle Bay, and CB6.3 and CB7.4 in the lower Bay. The results for Hurricane Floyd are shown on the left while those for Isabel are on the right, and the dashed lines denote the four-day window when local hurricane winds were imposed on the estuary. Several features can be noted immediately. First, despite the existence of spatial variability, it appears that a consistent Bay-wide sub-tidal velocity pattern emerges if one takes an ensemble across all five stations. Fig. 17 is a schematic drawing of the distinct two-pulse pattern that is revealed. For Hurricane Floyd, it shows that the surface current initially flows seaward followed by a landward flow, whereas for Hurricane Isabel, the surface current initially flows landward followed by a seaward flow. This two-pulse feature is closely associated with the sea level adjustment of the estuary to the local wind forcing; for Hurricane Floyd, the onset of down-estuary wind generates a down-estuary net volume transport and, at the end of the event, the sea level relaxes; for Hurricane Isabel, the onset of wind is up-estuary, and volume transport is up-estuary. This is consistent with the findings of CS, in that the two-pulse feature is a basic pattern of an estuary responding to the steady local wind forcing involving an exchange flow. Given that the present study is conducted using the actual Bay geometry and under strongly unsteady wind conditions during a hurricane, there are, however, significant differences between our results and those of CS. For example, the large sub-tidal velocity pulses, at the Bay mouth for Hurricane Floyd and in the upper Bay for Hurricane Isabel, deviate substantially from a symmetric two-pulse pattern. Furthermore, if one connects the largest sub-tidal velocity in each time series from the lower Bay to the upper Bay, as shown by the green line in Fig. 16, a clear

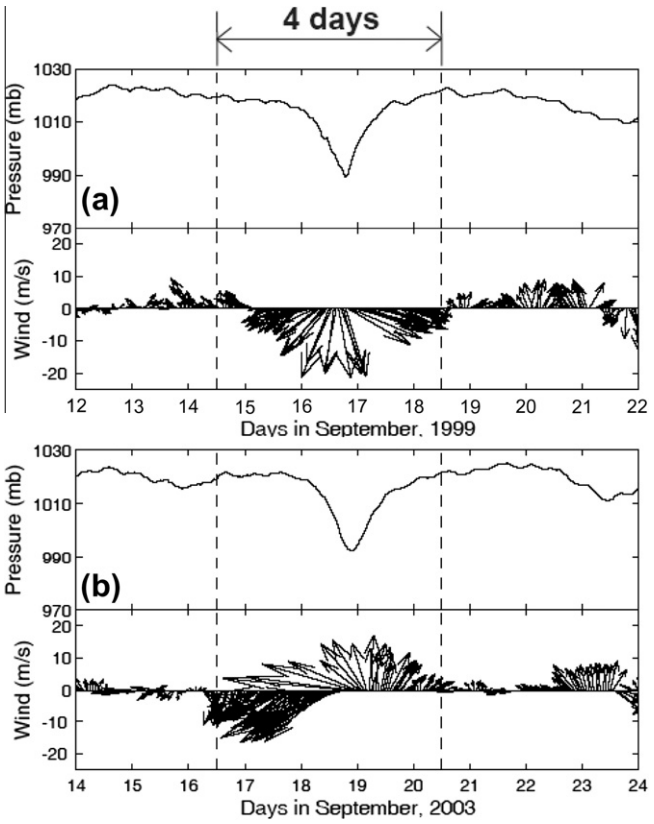

Fig. 15. Atmospheric forcing for four-day period during Hurricane Floyd (a) and Hurricane Isabel (b).

disturbance can be seen in the propagation pattern along the time versus space domain. This suggests that the forced long wave induced by the propagation of a storm plays an important role in shaping the transient response of the Bay to the hurricane forcing.

Fig. 18 shows the salinity response to the local wind. The response during Hurricane Floyd (left) is different from that during Hurricane Isabel (right), as the sub-tidal salinity has a major drop during Floyd, whereas it increased during Isabel. These large variations of sub-tidal salinity are associated with the disturbances propagating down and up the Bay, and are similar to those which were observed in the sub-tidal velocity time series. For the case of Hurricane Floyd, the disturbance propagates from the upper to the lower Bay with a decrease of salinity, whereas, for the case of Hurricane Isabel, the disturbance propagates from the lower to the upper Bay associated with an increase in the salinity. A mechanism that elucidates the time-dependent response of a propagating storm is critically important in future research, as hurricane winds are notoriously unsteady. In Fig. 19, we also show the vertical profiles of sub-tidal salinity in the lower, middle, and upper Bay as a time sequence. The time t1 is shown as the initial profile, t2 is the onset of strong winds, and t3 is the end of the event. It can be seen that the profile in the lower Bay after the onset of the wind event is more vertically well-mixed than that in the middle Bay. Hansen and Rattray (1965) indicated that the exchange flow is inversely proportional to the vertical mixing, and thus gave us a clue as to what to expect for the vertical profile of the sub-tidal velocity. Indeed, the profile in the middle Bay showed a clear shear flow pattern, with much stronger landward flow at the bottom layer, whereas, in the lower Bay, the velocity profile is generally more oscillatory across the two sides of the initial profile.

5.2. Variability of mixing regimes under down-estuary wind

One of the hallmarks of an estuary's response to a down-estuary wind is that it can encounter a number of regimes, from wind-induced straining to complete turbulent mixing, when the wind changes from moderate to strong. We have two cases to demonstrate this: Fig. 16(e) and Fig. 18(e) show the time series of velocity and salinity in the lower Bay during Hurricane Floyd. Between days 186–188, when there is a moderate down-estuary wind, it is shown that the sub-tidal velocities vary slightly between landward and seaward and the stratification of salinity increases, an indication of wind-induced straining. However, at the onset of a strong down-estuary wind at day 189.5, the velocity becomes seaward and the salinity drops by almost 10 ppt at the surface and bottom, becoming completely mixed. The regime obviously changes to a turbulent mixed condition. Given a constant wind, this variation of the regime can also occur spatially if the parameter characterizing the mixed layer depth, h_s/H, goes above the threshold value of 0.5 (where h_s is the mixed layer depth and H is the total depth). In Fig. 19(b), the vertical profile of sub-tidal velocity is shown along with the vertical profile of salinity. The time t0–t2 corresponds to moderate wind, the time t3–t6 corresponds to the strong wind, and time t7 corresponds to the end of the event in the lower, middle, and upper portions of the Bay. The value of h_s/H was estimated based on the salinity profile before the onset of the strong wind at time t3. It is obvious that h_s/H takes its largest value in the lower Bay, followed by the upper Bay, and that the middle Bay has the smallest value, partly due to the deep basin in this region. The smaller the value of h_s/H, the shallower is the mixed layer and the less mixing has occurred. The response of the velocity profile (on the left panel) to the down-estuary wind in the middle Bay shows that, for most of the time, it was landward with a vertical shear (an indication of a wind-straining regime), whereas in the lower and upper portions of the Bay, the velocity profile oscillates between seaward and landward directions without much of a vertical shear (an indication of the presence of a well-mixed regime).

With the above analysis, it is natural to ask if one can describe the interaction between the straining and mixing to form a parameter to represent the wind-induced variations in stratification. CS has defined the modified horizontal Richardson number, which is combined with the Wedderburn number (W), as:

$$(Ri_{x,CS})^2 = \frac{(H^4 N_x^4/48K_M)(1-W)}{R_f(u_{*S}^3/kh_S + u_{*B}^3/kh_B)} \tag{9}$$

where N_x ($\approx g\beta\Gamma$) is the horizontal buoyancy frequency, K_M is the effective vertical eddy viscosity (Dyer, 1997), and u_{*S} and u_{*B} are the root-mean-square values of friction velocities on the surface and bottom layers, respectively. The surface and bottom boundary layer thickness (h_S and h_B) are estimated by an entrainment model (Trowbridge, 1992; Chant et al., 2007):

$$h_S = \sqrt{2\gamma Ri_C^{1/2}\frac{u_{*S}^2}{N_\infty}\Delta t}, \quad h_B = \sqrt{2\gamma Ri_C^{1/2}\frac{u_{*B}^2}{N_\infty}\Delta t} \tag{10}$$

where γ is a constant (=1.22), Ri_c is the critical gradient Richardson number (=0.25), Δt is a characteristic time scale chosen as 3 h, and N_∞ represents background stratification. Following Ralston et al. (2008), K_M is assumed to scale as $a_0 C_d U_t \ell$, where $a_0 = 0.028$ and ℓ is a vertical mixing length scale. When the surface and bottom boundary layers merge ($h_S + h_B \geqslant H$), ℓ scales with H. Otherwise, the average of h_S and h_B is used for ℓ (CS, 2009). For values of $Ri_{x,CS}$ greater than a threshold value (of order 1), the water column should stratify, and for sub-critical values the water column should remain unstratified (Stacey et al., 2001).

The modified horizontal Ri in Eq. (9) was calculated at selected stations along the channel of the Bay during both hurricanes. The

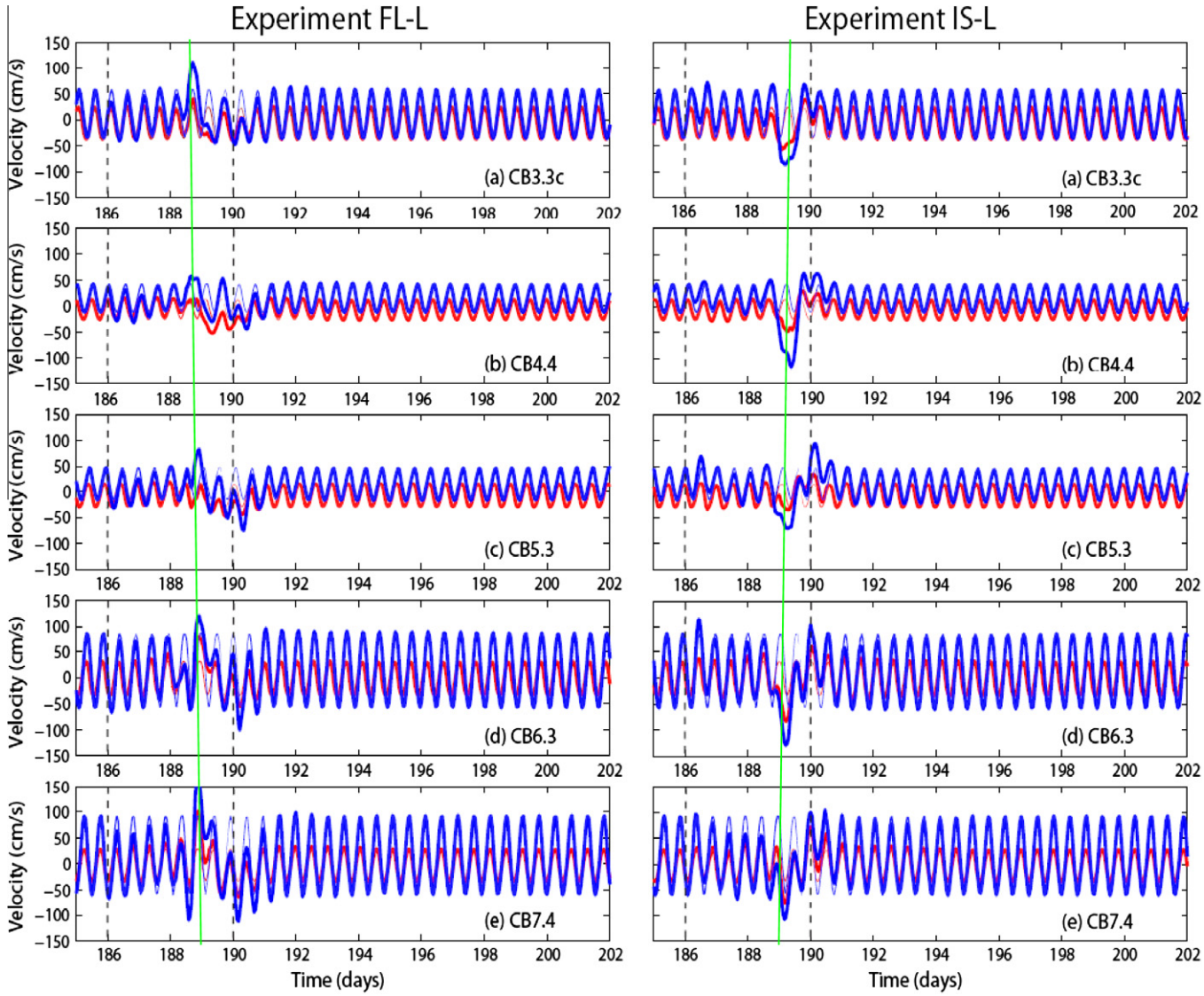

Fig. 16. Time series plots of surface (blue) and bottom (red) along-channel velocities at five selected stations for the cases of FL-L (left) and IS-L (right). Thin lines denote no wind case, vertical dashed lines denote the period of wind forcing, and positive value represents a seaward flow.

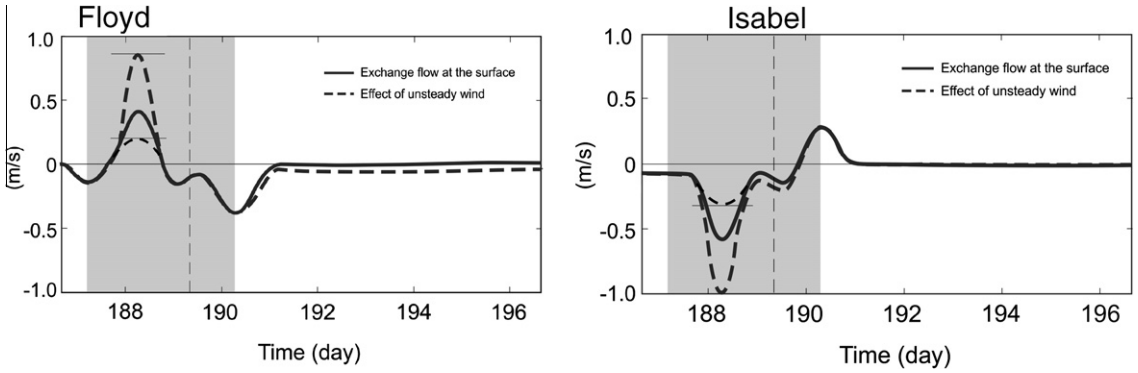

Fig. 17. A schematic pattern in exchange flow at the surface and effect of unsteady wind during Hurricanes Floyd (left) and Isabel (right).

temporal variation of $Ri_{x,CS}$ for three experiments is plotted in Fig. 20a. Without wind forcing, although $Ri_{x,CS}$ showed the tidal variability, the minimum values of $Ri_{x,CS}$ at the three locations were approximately 0.2, 1.0, and 0.3, respectively (Fig. 20a). This

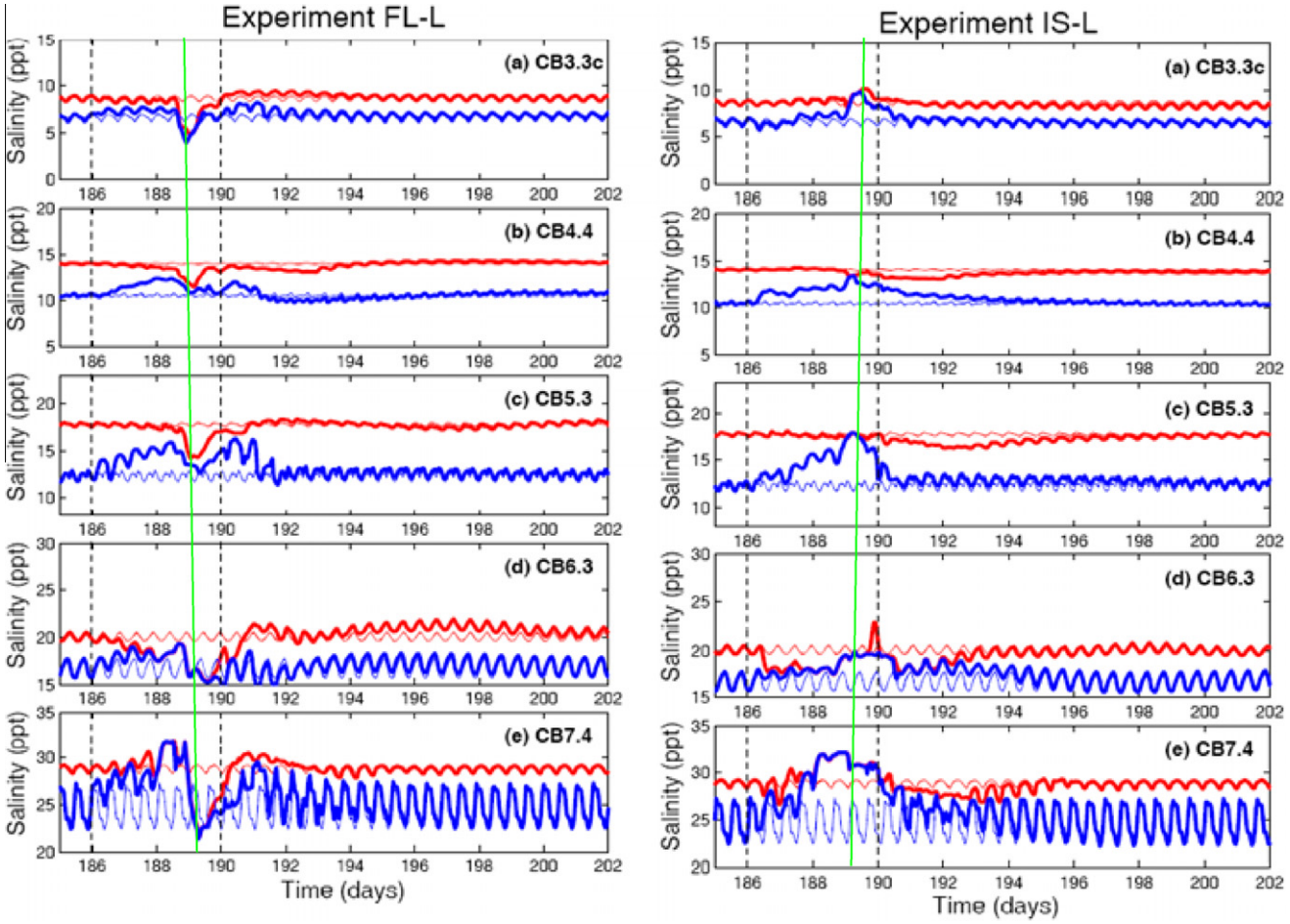

Fig. 18. Time series plots of surface (blue) and bottom (red) salinities at five selected stations for the cases of FL-L (left) and IS-L (right). Thin lines denote no wind case and vertical dashed lines denote the period of wind forcing.

indicates that tidally induced mixing dominates in the upper and lower Bay, whereas stratification is relatively significant in the mid Bay. In the case of Hurricane Floyd (Fig. 20a(d)–(f)), $Ri_{x,CS}$ decreased at all three locations. The value of $Ri_{x,CS}$ dropped below 0.1 in the upper and lower Bay, and reached a value of 0.25 in the mid-Bay. Interestingly, the value of $Ri_{x,CS}$ increased rapidly to greater than 1 in the upper and middle Bay regions. In the lower Bay, the value of $Ri_{x,CS}$ persisted below 0.1 for one day and then increased until the end of the Floyd wind period. The period of increase in the value of $Ri_{x,CS}$ appears to be consistent with the period of N_x increase due to down-Bay winds. This indicates that straining becomes important when down-Bay winds diminish. In the IS-L case (Fig. 20a(g)–(i)), $Ri_{x,CS}$ gradually began to decrease and rapidly dropped below 0.1 at all three locations. The low value of $Ri_{x,CS}$ persisted until the Isabel wind period ended. This indicates that the expansion of N_x was restricted by the up-estuary winds until the end of the Isabel wind period. The peaks of $Ri_{x,CS}$ between days 9 and 10 appear to occur when the landward flow changes to a seaward flow. The time series of the vertical distribution of eddy diffusivity were also generated for the 5 days event period in the upper, middle, and lower Bay, as shown in Fig. 20b. The unit of eddy diffusivity is m^2/s and was plotted in $\log_{10}$ scale in order to cover its wide-range of the values. It is interesting to note that the bottom half of the water in the middle portion of the Bay did not completely mix even under the assault of the Hurricane events. This is consistent with the results shown in Fig. 20a in that the mid-Bay deep channel is the most resilient spot to the vertical mixing. On the other hand, the lower Bay was well-mixed from top to bottom during the peak of the storm in both events with the corresponding eddy diffusivity as high as 10^{-1} m^2/s. The Upper Bay was shallow, but maintained a certain degree of stratification during the hurricane, probably due to the freshwater inflow and restriction of the fetch distance for the wind by the surrounding landmass. The re-stratification after the hurricane event was much stronger for Hurricane Isabel than that for Hurricane Floyd, presumably due to the fact that hurricane Isabel moved a significant amount of salty water landward and that, in turn, re-established the estuarine gravitational circulation faster.

6. Influence of the precipitation on salinity rebound

One of the effects observed during Hurricane Floyd was its unusually large precipitation (~1 inch/h) discharged directly onto the Bay water, which was recorded at Norfolk, VA. From a numerical modeling point of view, the precipitation acted like a point source and can be expressed as:

$$\frac{\partial \eta}{\partial t} + \nabla \cdot \int_{-h}^{\eta} \vec{u} dz = R \tag{11}$$

where R ($=Q_R/A$) is added to the right hand side of the continuity equation as a point source.

Based on this record, R [$m\,s^{-1}$] was determined as a surface boundary condition in the model to allow the mass and

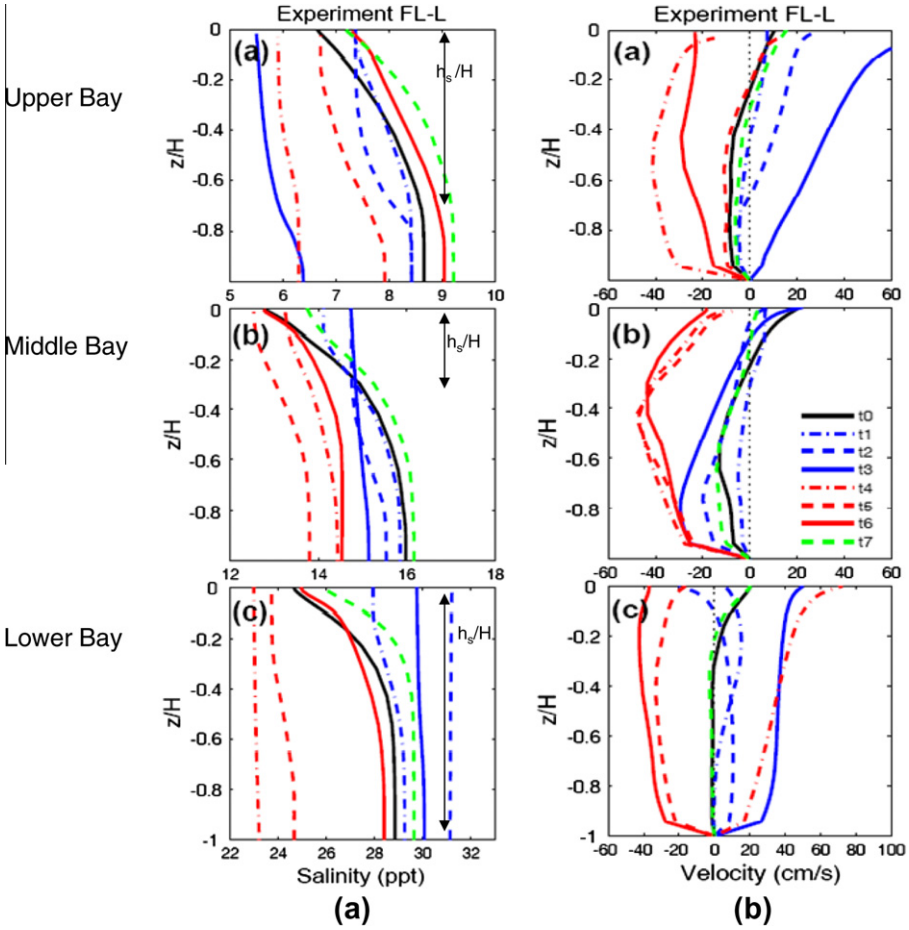

Fig. 19. Vertical profiles of tidally averaged salinity (left) and along-channel velocity (right) at three stations with time sequence: upper Bay (top); mid Bay (middle); lower Bay (bottom) for the case of FL-L. The positive value in velocity represents a seaward flow.

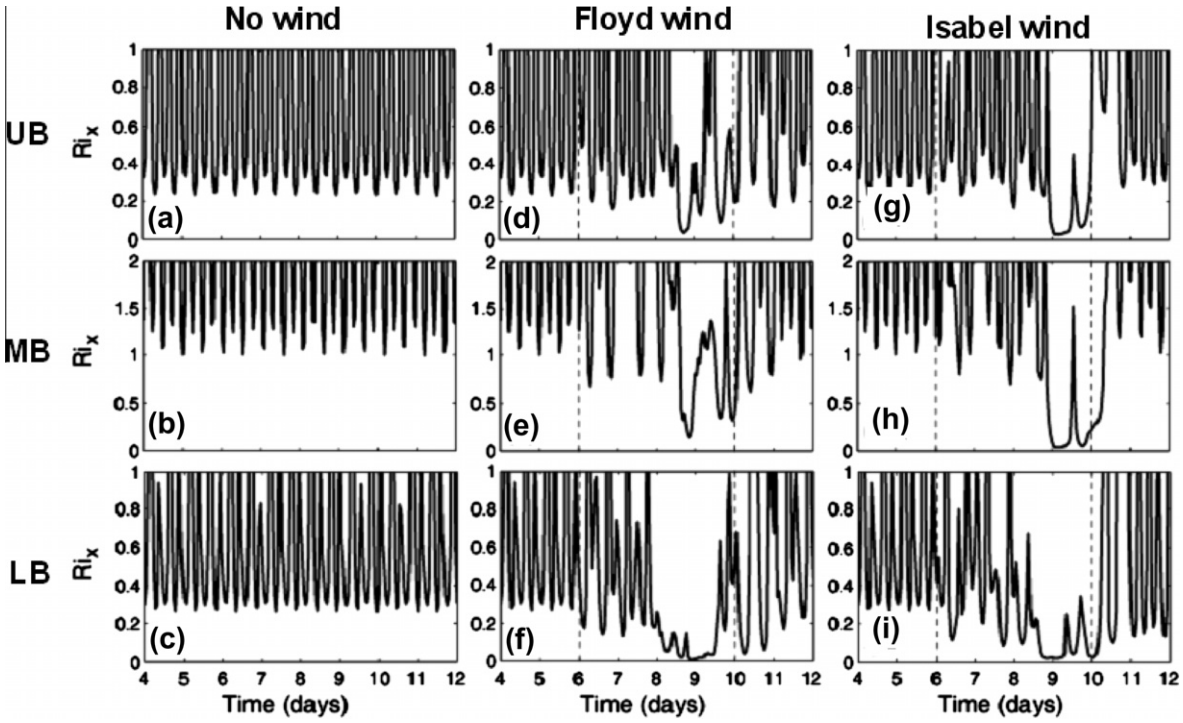

Fig. 20a. Temporal variations of the horizontal Richardson number ($Ri_{x,CS}$) at three locations for the cases of NW, FL-L, and IS-L.

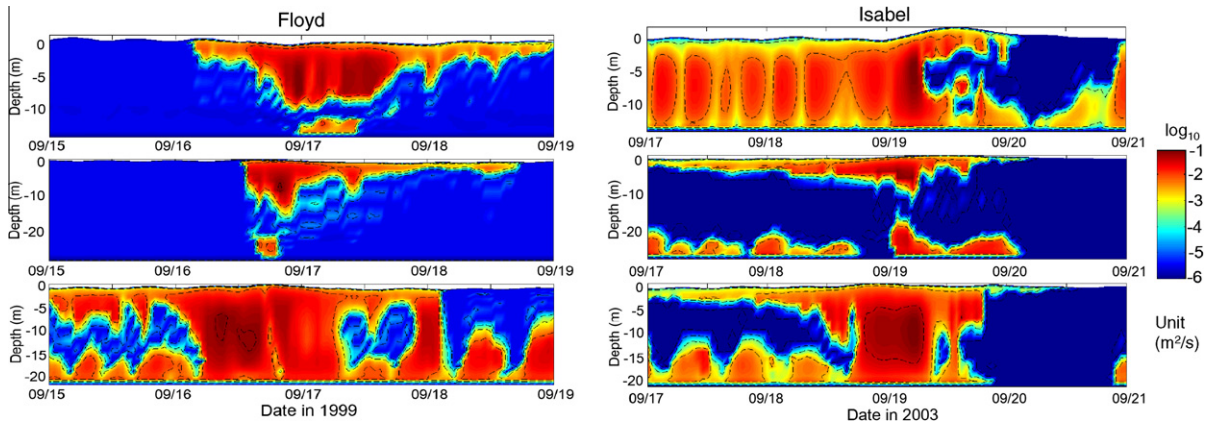

Fig. 20b. Temporal variations of the vertical eddy diffusivity at three locations for the cases of FL-L and IS-L, shown in Fig. 20. The unit of the eddy diffusivity is m^2/sec and the color bar is shown on a $\log_{10}$ scale.

momentum from precipitation to transfer through the water surface. The velocity and volume flux obtained in the momentum equations are then used in the salt balance equation.

Without precipitation, although the model reproduced rapid salinity decreases at two stations near the Bay mouth, the predicted salinity rapidly rebounded within two days, showing approximately 5 ppt of difference from the observed salinity, as shown by the thin line in Fig. 21. To improve the accuracy of the model for salinity, the methods described above were applied to the model by using the precipitation record of the Norfolk Airport. The model result without precipitation failed to reduce the 5-ppt difference, whereas the second method incorporating Eq. (11) reproduced the observed salinity, as shown in Fig. 21 by the thick solid line. An additional model test was performed by prescribing precipitation over the entire domain including the continental shelf. The results in this case were not much different from the previous test where the precipitation was only prescribed within the Bay. The model results indicate that the seaward horizontal barotropic pressure gradient induced by precipitation plays a role in retarding the salinity rebound after the salinity rapidly dropped. To improve model accuracy, the spatial distribution of precipitation input based on observation records is suggested for future model simulation of hurricanes.

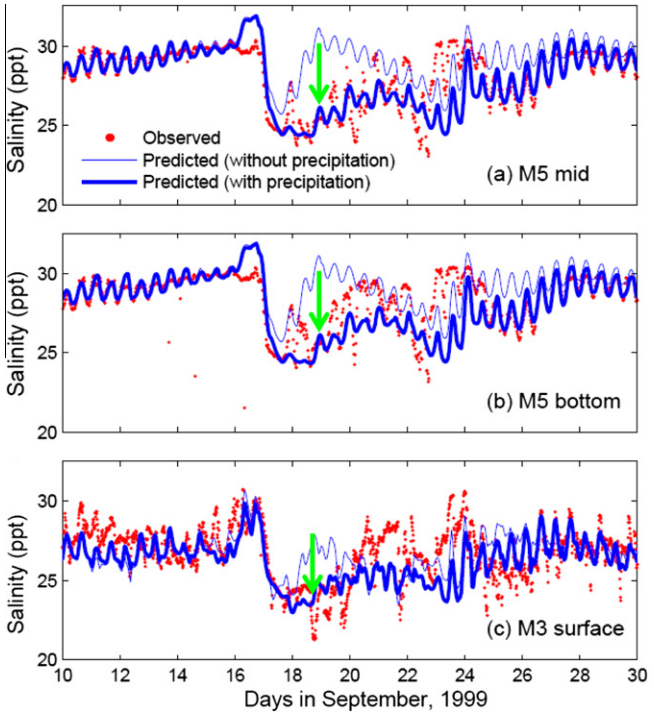

Fig. 21. Same as Fig. 9 except for comparing two experiments without precipitation (thin solid line) and with precipitation (thick solid line). Green arrows represent the decrease of salinity.

7. Conclusions

The response of Chesapeake Bay to forcing from two hurricanes is investigated using an unstructured-grid three-dimensional hydrodynamic model SELFE. The hurricanes chosen for the study are Hurricane Floyd (1999) and Hurricane Isabel (2003), both of which made landfall within 100 km of the mouth of the Bay. The two hurricanes differ in track, strength, translation speed, and precipitation pattern, but the model catches the major features of both events. The model results agree reasonably well with field observations of water level, velocity, and salinity. From the Bay's water level response to the hurricanes, it was found that the storm surge has two distinct stages: an initial stage set up by the remote winds and the second stage - a primary surge induced by the local winds. For the initial stage, the rising of the coastal sea level was setup by the remote wind of both hurricanes similarly, but for the second stage, the responses to the two hurricanes' local winds are significantly different. Hurricane Floyd was followed by down-Bay winds that canceled the initial setup and caused a set-down from the upper Bay. Hurricane Isabel, on the other hand, was followed by up-Bay winds, which reinforced the initial setup and continued to rise up against the ahead of the upper Bay. The volume flux were estimated at multiple cross-sectional transects throughout the Bay, and it was found consistently from each transect that the net outflow dominated during Hurricane Floyd while the net influx dominated during Hurricane Isabel. The oceanic influxes of water volume and salt flux were setup by the remote winds from the continental shelf into the Bay in the initial stages of the hurricanes. As the hurricanes approached close to the shore, the local wind became more significant. When the hurricanes made landfall, the strong local surface wind stress dominated and was the primary agent in destratifying the water column through transferring turbulent kinetic energy from the surface to the lower layer of the Bay. The model simulation indicated that large volume and salt

fluxes in the form of sub-tidal velocity and down-gradient salt flux were found to move up the Bay in the case of Hurricane Isabel and down the Bay in the case of Hurricane Floyd. A controlled experiment was conducted and demonstrated that down-Bay winds of an eastern-track hurricane tend to enhance stratification under moderate winds, but exhibit an increasing-then-decreasing variability when the wind stress increases. The up-Bay winds of a western-track hurricane tend to reduce the stratification with the generation of a deeper mixed layer. A modified horizontal Richardson number that incorporated the wind stress, wind direction, horizontal salinity gradient, and vertical eddy viscosity, represented the stratified–destratified conditions reasonably well for the wind-induced straining as well as the vertical mixing processes during hurricane events. In addition, the precipitation associated with the hurricane acted as a point source of water mass on the surface of water, which not only diluted surface water but also generated a seaward barotropic horizontal pressure gradient. This overwhelmed the baroclinic pressure gradient and was shown in the model simulation to affect the subsequent redistribution of salinity after the storm.

Acknowledgements

The present study was carried out as part of the Chesapeake Bay Inundation Prediction System (CIPS) funded by NOAA IOOS Program through Southeastern Universities Research Association Coastal Ocean Observing and Prediction Program. We also greatly appreciate Dr. William Boicourt of Horn Point Laboratory, University of Maryland for sharing the velocity measurements conducted during Hurricane Isabel.

References

Austin, J.A., 2002. Estimating the mean ocean-bay exchange rate of the Chesapeake Bay. Journal of Geophysical Research 110, 3192.

Bills, P.J., 1991. Barotropic depth-averaged and three-dimensional tidal programs for shallow seas. PhD thesis, The University of Adelaide. South Australia. Department of Applied Mathematics.

Boicourt, W.C., 1973. The circulation of water on the continental shelf from Chesapeake Bay to Cape Hatteras. Ph.D. Dissertation. The Johns Hopkins University, Baltimore, MD, p. 183.

Boicourt, W.C., 2005. Physical response of Chesapeake Bay to hurricanes moving to the wrong side: Refining the forecasts. In: Sellner, K.G. (Ed.): Hurricane Isabel in Perspective. Chesapeake Research Consortium, CRC Publication 05-160, Edgewater, MD, pp. 39–48.

Brasseur, L.H., Trembanis, A.C., Brubaker, J.M., Friedrichs, C.T., Nelson, T., Wright, L.D., Haas, L.W., 2005. Physical response of the York River estuary to Hurricane Isabel. In: Sellner, K.G. (Ed.), Hurricane Isabel in Perspective. Chesapeake Research Consortium, CRC Publication 05-160, Edgewater, MD, pp. 57–63.

Bretherton, F.P., Davis, R.E., Fandry, C.B., 1976. A technique for objective analysis and design of oceanographic experiments applied to MODE-73. Deep-Sea Research 23, 559–582.

Burla, M., Baptista, A.M., Zhang, Y., Frolov, S., 2010. Seasonal and interannual variability of the Columbia River plume: A Perspective enabled by multi-year simulation databases. Journal of Geophysical Research 115, 25.

Carter, G.S., Merrifield, M.A., 2007. Open boundary conditions for regional tidal simulations. Ocean Modelling 18, 194–209.

Carter, H.H., Pritchard, D.W., 1988. Oceanography of Chesapeake Bay. In: Kjerfe, B. (Ed.), Hydrodynamics of Estuaries: Dynamics of Partially Mixed Estuaries, vol. 1. CRC Press, Boca Raton, FL, pp. 1–16.

Chant, R.J., Geyer, W.R., Houghton, R., Hunter, E., Lerczak, J.A., 2007. Estuarine boundary layer mixing processes: Insights from dye experiments. Journal of Physical Oceanography 37, 1859–1877.

Chen, S.N., Sanford, L.P., 2009. Axial wind effects on salinity structure and longitudinal salt transport in idealized, partially-mixed estuaries. Journal of Physical Oceanography., 1905–1920. http://dx.doi.org/10.1175/2009JPO4016.1.

Cho, K.-H., 2009. A numerical modeling study on barotropic and baroclinic responses of the Chesapeake Bay to hurricane events. Ph.D. Dissertation, The College of William and Mary, Williamsburg, VA.

Chesapeake Bay Program (CBP), 1993. Guide to using Chesapeake Bay Program water quality monitoring data. CBP/TRS 78/92, Chesapeake Bay Program, Annapolis, Maryland, p. 127.

Dyer, K.R., 1997. Estuaries: A Physical Introduction, 2nd ed. John Wiley and Sons, pp. 195.

Flather, R.A., 1976. A tidal model of the north-west European continental shelf. Smooth interpolation for large sets of scattered data. International Journal for Numerical Methods in Engineering 15, 1691–1704.

Franke, R., Nielson, H., 1980. Smooth interpolation for large sets of scattered data. International Journal for Numerical Methods in Engineering 15, 1691–1704.

Geyer, W.R., 1997. Influence of wind on dynamics and flushing of shallow estuaries. Estuarine, Coastal and Shelf Science 44, 713–722.

Goodrich, D.M., Boicourt, W.C., Hamilton, P., Pritchard, D.W., 1987. Wind-induced destratification in Chesapeake Bay. Journal of Physical Oceanography 17, 2232–2240.

Guo, X., Valle-Levinson, A., 2007. Tidal effects on estuarine circulation in Chesapeake Bay. Continental Shelf Research 27, 20–42.

Guo, X., Valle-Levinson, A., 2008. Lateral structure of wind effects on density-driven flow in the Chesapeake Bay. Continental Shelf Research 28, 2450–2471.

Hansen, D.V., Rattray, M., 1965. Gravitational circulation in straits and estuaries. Journal of Marine Research 23, 104–122.

Hicks, S.D., 1964. Tidal wave characteristics of Chesapeake Bay. Chesapeake Science 5, 103–113.

Holland, G.J., 1980. An analytic model of the wind and pressure profiles in hurricanes. Monthly Weather Review 108, 1212–1218.

Janowitz, G.S., Pietrafesa, L.J., 1996. Subtidal frequency fluctuations in coastal sea level in the Mid and South Atlantic Bights: A prognostic for coastal flooding. Journal of Coastal Research 12, 79–89.

Jelesnianski, C.P., Chen, J., Shaffer, W.A., 1992. SLOSH: Sea, Lake, and Overland Surges from Hurricane. National Weather Service, Silver Springs, MD.

Krome, E.C., Corlett, C.A., 1990. Modeling of the Chesapeake Bay. CRC Publication, No. 131.

Kuo, A.Y., Park, K., 1992. Transport of hypoxic waters: an estuary-subestuary exchange. In: Prandle, D. (Ed.), Dynamic and Exchange in Estuaries and the Coastal Zone. American Geophysical Union, Washington DC, pp. 599–615.

Lerczak, J.A., Geyer, W.R., Chant, R.J., 2006. Mechanism driving the time-dependent salt flux in a partially stratified estuary. Journal of Physical Oceanography 36, 2296–2311.

Li, M., Zhong, L., Boicourt, W.C., Zhang, S., Zhang, D.-L., 2007. Hurricane-induced destratification and restratification in a partially mixed estuary. Journal of Marine Research 65, 169–192.

Liu, W., Chen, W., Kuo, J., Wu, C., 2008a. Numerical determination of residence time and age in a partially mixed estuary using three-dimensional hydrodynamic model. Continental Shelf Research 28, 1068–1088.

Liu, W., Chen, W., Kuo, J., 2008b. Modeling residence time response to freshwater discharge in a mesotidal estuary, Taiwan. Journal of Marine Systems 74, 295–314.

Mellor, G.L., Yamada, T., 1982. Development of a turbulence closure model for geophysical fluid problems. Reviews in Geophysics 20, 851–875.

North, E.W., Chao, S.-Y., Sanford, L.P., Hood, R.R., 2004. The influence of wind and river pulses on an estuarine turbidity maximum: Numerical studies and field observations in Chesapeake Bay. Estuaries 27, 132–146.

Osher, S., 1984. Riemann solvers, the entropy condition, and difference approximations. SIAM Journal on Numerical Analysis 21, 217–235.

Pore, N.A., 1960. Chesapeake Bay hurricane surges. Chesapeake Science 1, 178–186.

Pore, N.A., 1965. Chesapeake Bay extratropical storm surges. Chesapeake Science 6, 172–182.

Ralston, D.K., Geyer, W.R., Lerczak, J.A., 2008. Subtidal salinity and velocity in the Hudson River Estuary: Observations and modeling. Journal of Physical Oceanography 38, 753–770.

Reay, W.G., Moore, K.A., 2005. Impacts of Tropical Cyclone Isabel on shallow water quality of the York River estuary. In: Sellner, K.G. (Ed.): Hurricane Isabel in Perspective. Chesapeake Research Consortium, CRC Publication 05-160, Edgewater, MD, pp. 135–144.

Reid, R.O., 1990. Water level changes. Handbook of Coastal and Ocean Engineering. Gulf Publishing, Houston, Texas.

Rodi, W., 1984. Turbulence models and their applications in hydraulics: a state of the art review. Delft, The Netherlands. International Association for Hydraulics Research.

Roe, P.L., 1986. Characteristic-based schemes for the Euler equations. Annual Review of Fluid Mechanics 18, 337–365.

Roman, M.R., Adolf, J.E., Bichy, J., Boicourt, W.C., Harding Jr., L.W., Houdle, E.D., Jung, S., Kimmel, D.G., Miller, W.D., Zhang, X., 2005. Chesapeake Bay plankton and fish abundance enhanced by Hurricane Isabel. EOS 86, 261–265.

Scully, M.E., Friedrichs, C., Brubaker, J., 2005. Control of estuarine stratification and mixing by wind-induced straining of the estuarine density field. Estuaries 28, 321–326.

Seitz, R.C., 1971. Temperature and salinity distributions in vertical sections along the longitudinal axis and across the entrance of the Chesapeake Bay (April 1968 to March 1969). Chesapeake Bay Institute, The Johns Hopkins University, p. 99.

Shen, J., Gong, W., Wang, H., 2005. Simulation of Hurricane Isabel using the advanced circulation model (ADCIRC). In: Sellner, K.G. (Ed.), Hurricane Isabel in Perspective. Chesapeake Research Consortium, CRC Publication 05-160, Edgewater, MD, pp. 107–116.

Shen, J., Gong, W.P., Wang, H.V., 2006a. Water level response to 1999 Hurricane Floyd in the Chesapeake Bay. Continental Shelf Research 26, 2484–2502.

Shen, J., Wang, H., Sisson, M., Gong, W., 2006b. Storm tide simulation in the Chesapeake Bay using an unstructured grid model. Estuarine, Coastal and Shelf Science 68, 1–16.

Shepard, D., 1968. A two-dimensional interpolation function for irregularly spaced data. In: Proceedings of the 1968 23rd ACM National Conference, pp. 517–524.

Stacey, M.T., Burau, J.R., Monismith, S.G., 2001. Creation of residual flows in a partially stratified estuary. Journal of Geophysical Research 106, 17,013–17,037.
Sweby, P.K., 1984. High resolution schemes using flux limiters for hyperbolic conservation laws. SIAM Journal on Numerical Analysis 21, 995–1011.
Trowbridge, J.H., 1992. A simple description of the deepening and structure of a stably stratified flow driven by a surface stress. Journal of Geophysical Research 97, 15 529–15 543.
Umlauf, L., Burchard, H., 2003. A generic length-scale equation for geophysical turbulence models. Journal of Marine Research 61, 235–265.
Umlauf, L., Burchard, H., 2005. Second-order turbulence closure models for geophysical boundary layers. A review of recent work. Continental Shelf Research 25, 795–827.
Valle-Levinson, A., 1995. Observations of barotropic and baroclinic exchanges in the lower Chesapeake Bay. Continental Shelf Research 15, 1631–1647.
Valle-Levinson, A., Wilson, R.E., 1994. Effects of sill bathymetry, oscillating barotropic forcing and vertical mixing on estuary/ocean exchange. Journal of Geophysical Research 99, 5149–5169.
Valle-Levinson, A., Lwiza, K.M.M., 1997. Bathymetric influences on the lower Chesapeake Bay hydrography. Journal of Marine System 12, 221–236.
Valle-Levinson, A., Miller, J.L., Wheless, G.H., 1998. Enhanced stratification in the lower Chesapeake Bay following northeasterly winds. Continental Shelf Research 18 (13), 1631–1647.
Valle-Levinson, A., Wong, K.-C., Bosley, K.T., 2001. Observations of the wind-induced exchange at the entrance to a coastal plain estuary. Journal of Marine Research 59, 391–416.
Valle-Levinson, A., Wong, K.-C., Bosley, K.T., 2002. Response of the lower Chesapeake Bay to forcing from Hurricane Floyd. Continental Shelf Research 22, 1715–1729.
Valle-Levinson, A., Reyes, C., Sanay, R., 2003. Effects of bathymetry, friction, and rotation on estuary-ocean exchange. Journal of Physical Oceanography 33, 2375–2393.
Wang, D.-P., Elliott, A.J., 1978. Non-tidal variability in the Chesapeake Bay and Potomac River: evidence for non-local forcing. Journal of Physical Oceanography 8, 225–232.
Wang, H., Cho, J., Shen, J., Wang, Y.P., 2005. What has been learned about storm surge dynamics from Hurricane Isabel model simulation? In: Sellner, K.G. (Ed.), Hurricane Isabel in Perspective. Chesapeake Research Consortium, CRC Publication 05-160, Edgewater, MD, pp. 117–125.
Wilcox, D.C., 1998. Reassessment of scale determining equation for advance turbulence models. AIAA Journal 26, 1299–1310.
Zervas, C., Duncan, S., Deitemyer, D., Hubbard, J., Culp, J., Landon, T., Connolly, M., Wright, D., Bourgerie, R., 2000. Effects of Hurricane Floyd on water levels. NOAA Technical Report NOS CO-OPS 027, p. 109.
Zhang, Y.-L., Baptista, A.M., Myers, E.P., 2004. A cross-scale model for 3D baroclinic circulation in estuary-plume-shelf systems: I. Formulation and skill assessment. Continental Shelf Research 24, 2187–2214.
Zhang, Y., Baptista, A.M., 2008. A semi-implicit Eulerian–Lagrangian finite-element model for cross-scale ocean circulation. Ocean Modelling 21, 71–96.
Zhong, L., Li, M., 2006. Tidal energy fluxes and dissipation in the Chesapeake Bay. Continental Shelf Research 26, 752–770.